Recent progress on quantum dot solar cells: a review

Tomah Sogabe
Qing Shen
Koichi Yamaguchi

Recent progress on quantum dot solar cells: a review

Tomah Sogabe,[a,b] **Qing Shen,**[a,b] **and Koichi Yamaguchi**[a,b,*]

[a]University of Electro-Communications, Info-Powered Energy System Research Center,
1-5-1 Chofugaoka, Chofu, Tokyo 182-8585, Japan
[b]University of Electro-Communications, Department of Engineering Science,
1-5-1 Chofugaoka, Chofu, Tokyo 182-8585, Japan

Abstract. Semiconductor quantum dots (QDs) have a potential to increase the power conversion efficiency in photovoltaic operation because of the enhancement of photoexcitation. Recent advances in self-assembled QD solar cells (QDSCs) and colloidal QDSCs are reviewed, with a focus on understanding carrier dynamics. For intermediate-band solar cells using self-assembled QDs, suppression of a reduction of open circuit voltage presents challenges for further efficiency improvement. This reduction mechanism is discussed based on recent reports. In QD sensitized cells and QD heterojunction cells using colloidal QDs well-controlled heterointerface and surface passivation are key issues for enhancement of photovoltaic performances. The improved performances of colloidal QDSCs are presented. © *The Authors. Published by SPIE under a Creative Commons Attribution 3.0 Unported License. Distribution or reproduction of this work in whole or in part requires full attribution of the original publication, including its DOI.* [DOI: 10.1117/1.JPE.6.040901]

1 Introduction

Semiconductor quantum dots (QDs) have drawn considerable interest for more than 20 years because of the optoelectronic advantages based on a zero-dimensional system. The photovoltaic applications using self-assembled quantum dots (SAQDs) and colloidal quantum dots (CQDs) have the potential to enhance the photogeneration of carriers through the QD energy level or band.[1–5] An increase in the maximum attainable thermodynamic conversion efficiency is theoretically predicted by expanding the available spectrum for the photoexcitation. However, the fundamental physics of carrier transport and carrier collection must be considered for the real photovoltaic operation. Understanding of their basic photovoltaic mechanisms in SAQDs and CQDs is essential to a design of ideal solar cell structures having high power conversion efficiency (PCE). Additionally, technical progress in the growth of SAQDs and the synthesis of CQDs is most important to construct the realistic solar cell structures, which include appropriate materials with high crystal quality, well-controlled heterointerface, and surface passivation. The recent progress in SAQD solar cells and CQDSCs is remarkable. Consequently, for their future prospects, it is significant to discuss their improved properties and current problems.

Recently, several papers on QDSCs, which were specialized in either SAQDs or CQDs, have been published. For III-V compounds, such as InAs/GaAs SAQDSCs, Okada et al.[6] have reviewed the latest progress on intermediate band solar cells (IBSCs) focused on the thermodynamics of solar energy conversion, the device physics, and the two-step intersub-band absorption/recombination. Wu et al.[7] have summarized recent developments in QD optoelectronic devices, including 1.3-μm-wavelength QD lasers, QD infrared photodetectors, and QD-IBSCs. Zheng et al.[8] reviewed the recent progress in QDSC, especially on the enhanced optical absorption. On the other hand, for CQD-based solar cells, Kramer and Sargent[9] have thoroughly reviewed the architecture of CQDSCs with special focus on the material and device.

*Address all correspondence to: Koichi Yamaguchi, E-mail: kyama@ee.uec.ac.jp

Duan et al.[10] have reviewed the recent advance in materials for QD-sensitized solar cell application. Wang[11] reviewed the device physics in CQDSC. In this paper, we united highlights of more recent advances in both SAQDSCs and CQDSCs. The main subject of this review is recent experimental results and understanding of carrier dynamics in both solar cell operations.

In SAQD-SCs (Chapter 2), we focus on IBSCs with SAQDs. The IBSC was proposed as a way of breaking the detailed balance efficiency limits of conventional single gap solar cells.[1] The fundamental operation of the IBSC is based on two-step photoexcitation of carriers from a valence band to a conduction band via a miniband of coupled QDs, which is located within a band gap of the host material. Although the two-step photoexcitation enhances photocurrent, an open-circuit voltage (V_{oc}) often decreases. According to theoretical calculations using a detailed balance model, a large QD number of more than 3×10^{13} cm^{-2} and high concentrated sunlight are needed to achieve high PCE.[12–14] To prepare the ultrahigh-density QDs with an electronic coupling, stacking growth[15–21] and in-plane high-density growth[22,23] techniques have been developed. Recently, many researchers are attempting to explain the experimental results of QD-IBSCs by a more realistic model, including various processes: photoexcitation, carrier separation, carrier transport, and recombination. Therefore, we review such carrier dynamics in the QD-IBSC operation in this chapter.

The state-of-the-art photovoltaic devices using CQDs are presented in Chapter 3. The most common approach to the synthesis of CQDs is the controlled nucleation and growth of nano-particles in a chemical solution of precursors containing the metal and anion sources. Such a convenient method has many advantages for utilizing various materials and reducing the process cost.[24,25] In this chapter, recent progress in CQD-sensitized solar cells and CQD heterojunction solar cells (HSCs) is reviewed briefly. In particular, the PCE of CQDSCs improved remarkably in the last several years. The carrier dynamics including photogeneration, spatial separation, transfer, and recombination are key issues for increasing the efficiency. Recently, development of well-controlled heterointerface and effective surface passivation is pushed forward to suppress the undesired carrier recombination and enhance the carrier transport.

2 InAs/GaAs Quantum Dot Solar Cell: Effect of Carrier Dynamics on V_{oc}

2.1 Introduction

The issue that has received the most attention in recent InAs/GaAs QDSC research is the reduction of the V_{oc} when compared to the GaAs control cell.[26–31] Experimentally confirmed short circuit currents J_{sc} for both GaAs- and InAs QD-based solar cells are almost identical (note: Some InAs /GaAs QDSC showed slightly higher J_{sc} than GaAs SC, but the increase amount is fairly small and usually <0.5 mA/cm^2).[15,32–35] Under such a situation, the lower V_{oc} observed in QDSC was attributed mainly to the larger dark recombination current when compared to GaAs control cell. To understand the dark recombination current in QDSC, modeling of the carrier dynamics is indispensable.[6,36–38] A simplified two-voltage region model is proposed by us, as shown in in Figs. 1(a)–1(c).[39,40]

For a p-i-n type QDSC under low forward bias voltage [see Fig. 1(b)], the voltage is mainly applied across the space charge region (SCR). For the recombination behavior within this region, the dark current for GaAs and InAs/GaAs QDSC is described using a two-diode model as follows:

GaAs SC:

$$J_{\text{dark}}(V_{\text{low}}) = J_{0\text{SRH},i-\text{region}} \exp\left(\frac{qV}{2kT}\right) + J_{0,i-\text{region}} \exp\left(\frac{qV}{kT}\right), \tag{1}$$

InAs/GaAs QDSC:

$$J_{\text{dark}}(V_{\text{low}}) = J_{0\text{SRH},i+\text{QD region}} \exp\left(\frac{qV}{2kT}\right) + J_{0,i+\text{QD region}} \exp\left(\frac{qV}{kT}\right), \tag{2}$$
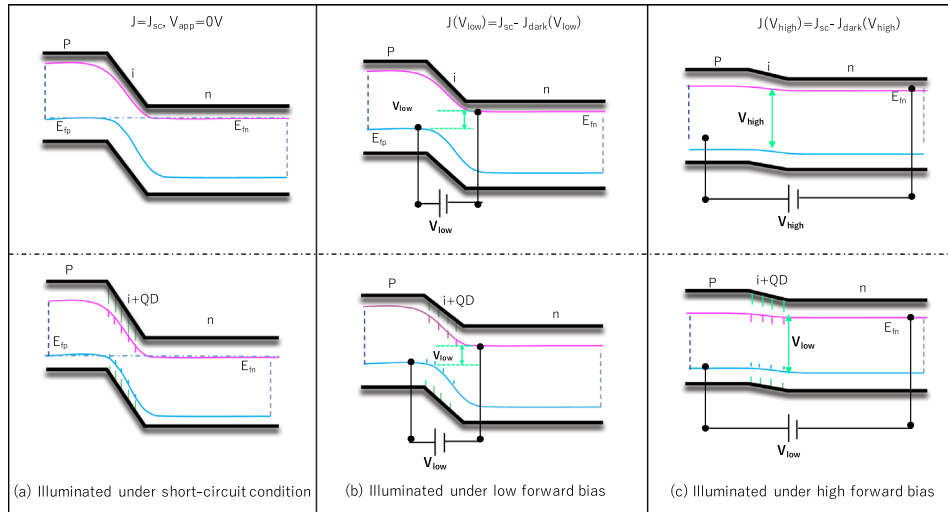
Fig. 1 Sketched band diagrams for GaAs SC and InAs/GaAs QDSC under (a) short-circuit condition, (b) low forward bias, and (c) high forward bias conditions.

where the J_{0SRH} is the Shockley–Read–Hall (SRH) recombination dark saturation current, and its magnitude is usually proportional to the density of defects.[28] On the other hand, J_0 is the radiative or diffusion recombination dark saturation current, and its magnitude is basically related to the material properties such as bandgap (the lower the bandgap, the higher the J_0) and diffusion length (the shorter diffusion length, the higher the J_0).[37,40,41] The generation of defects is usually more enhanced for the InAs QDs-embedded GaAs because of the accumulated strain compared with the i-GaAs layer without QDs, which inevitably cause the increase of J_{0SRH} and the decrease of V_{oc}.

When the p-i-n solar cell is under high forward bias [see Fig. 1(c)], the SCR region becomes negligible and the voltage drop is applied equally across the whole device; the dark currents for GaAs SC and InAs/GaAs QDSC are described as follows:

GaAs SC:

$$J_{dark}(V_{high}) = J_{0,pn} \exp\left(\frac{qV}{kT}\right) + J_{0,i-GaAs} \exp\left(\frac{qV}{kT}\right), \tag{3}$$

InAs/GaAs QDSC:

$$J_{dark}(V_{high}) = J_{0,pn} \exp\left(\frac{qV}{kT}\right) + J_{0,i+QD} \exp\left(\frac{qV}{kT}\right). \tag{4}$$

It can be seen from here that the total dark current in the InAs/GaAs QDSC might be higher than the GaAs SC due to the increased $J_{0,i+QD}$ caused by the reduced effective E_g in the QD region, thus causing the reduction of V_{oc}.

The reduction of V_{oc} in InAs/GaAs QDSC has recently become a central issue for further efficiency improvement. In this review, we have limited our focus on the works that have mainly dealt with interplay between carrier dynamics and device performance. Meanwhile, to ensure timeliness and currency, the works reviewed here were sorted and scrutinized from the literatures published in the past 2 to 3 years. The model described in this section will act as a supportive guide to better interpret the results summarized from the reviewed papers.

2.2 Carrier Escape Nature and Electric Field Effect

The photoelectrons generated by InAs QD light absorption usually, at first, have to escape from the potential formed between InAs QD and GaAs buffer. Understanding the carrier escape mechanism is crucial to further improving the device performance.[42,43] Sellers et al.[42] have
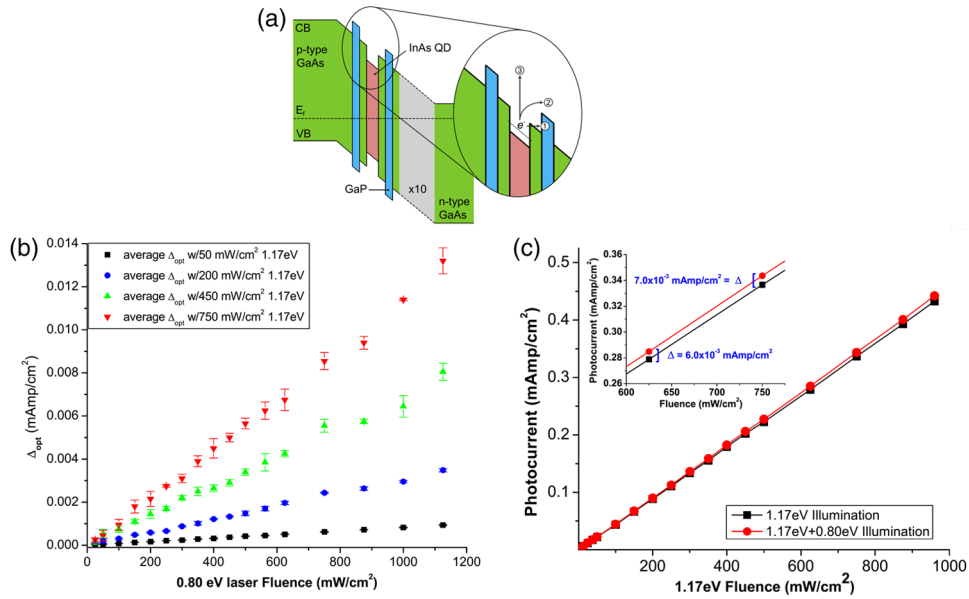
Fig. 2 (a) Schematic of the InAs/GaAs p-i-n junction solar cell device band gap structure. (a) The carrier escape pathways following InAs QD excitation (pathway 1, tunneling escape; pathway 2, thermal escape; and pathway 3, optically driven escape) are shown. (b) Photocurrent as a function of 1.17 eV illumination fluence with and without the addition of 600 mW/cm^2 0.80 eV light. (c) Change in photocurrent with the addition of 0.80 eV light to 1.17 eV illumination. Reprinted with permission from Ref. 42. © 2014 AIP Publishing LLC.

evaluated the carrier escape mechanism in InAs/GaAs QDSC by using photocurrent measurements under sub-bandgap illumination. The 1.17-eV photon source and 0.8-eV photo source were chosen, and their fluencies were varied to reveal the fundamental carrier escaping principle. The inset Fig. 2(a) depicts the three competing mechanisms for carrier extraction from intermediate states in QD: tunneling (pathway 1), thermal (pathway 2), and optically driven (pathway 3).[37,44] When the sample was solely under illumination of a 1.17-eV photon source, photocurrent was found to increase linearly with laser fluence over the range of fluences studied, as shown in Fig. 2(b). The linear increase suggests that thermal and tunneling escape mechanisms dominate any carrier escape driven optically by 1.17-eV photons. The effect of adding a 0.8-eV photon source was presented in Fig. 2(c). Here, Δ_{opt} was used to describe the increased photocurrent due to the addition of 0.8-eV light. Again, they found that the Δ_{opt} value increased linearly with increasing 0.80-eV fluence under a fixed fluence value of 1.17-eV photon source. If the photocurrent was limited solely by the generation of carriers within the QDs, Δ_{opt} should become saturated for high fluences of 0.8-eV photons.[42] The absence of saturation under these conditions suggests that there is a continuous supply of carriers that can be optically excited by 0.8-eV photons. The authors have proposed a carrier "retrapping model" to explain the experimental results.[42] Based on this model, Δ_{opt} depends linearly on the fluence of 0.8-eV photons because the addition of an optical escape pathway reduces the mean time carriers spent in traps in either the QD or wetting layer and, therefore, increases the conductivity (therefore, the photocurrent) even for a fixed number of carriers.[30] It is worthwhile to mention here that in a recent work, Asahi et al.[45] have reported a saturation of two-step photocurrents. However, unlike the work reported here involving the two-step photoexcitation from valence band to intermediate states and from intermediate states to conduction band, Asahi et al.[45] observed the saturation by tuning "two-step" photoexcitation from valance band to conduction band and from intermediate states to conduction band.

Related to the dynamic nature of carrier escape and separation mechanism, it has been shown that the excitonic dynamics of electrons and holes could be responsible for the nonadditive behavior of the photocurrent contributed by the QDs in a QDSC.[37] This nonadditive characteristic was observed when the total photocurrent of the cell was much lower than the sum of
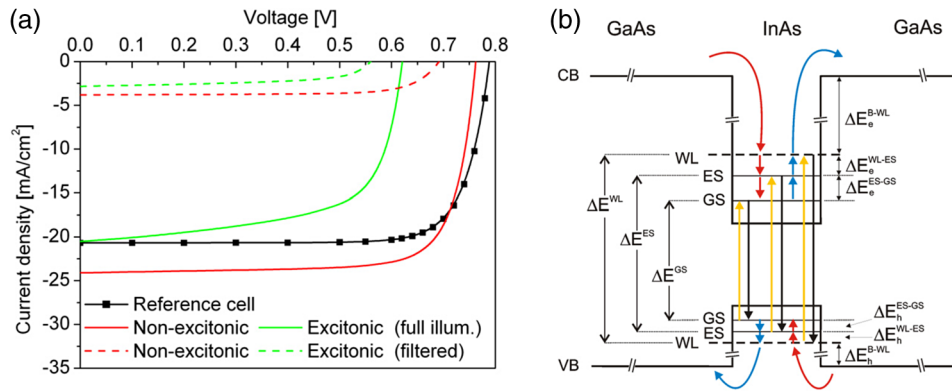
Fig. 3 (a) Energy band model of the InAs/GaAs system, as considered in this work. (b) $J - V$ characteristics of nonexcitonic and excitonic QDSCs, simulated under full (solid lines) and filtered ($\lambda > 870$ nm, dashed lines) AM1.5G solar spectrum illumination. The additive feature of the QD contribution can be inferred by observing the reference cell and QDSCs currents at short circuit. Reprinted with permission from Ref. 46. © 2016 IOP Publishing.

the photocurrents contributed by the barrier and the QDs separately, as reported for undoped InAs/GaAs solar cells.[46] Cedola et al.[46] have investigated the excitonic and nonexcitonic dynamic nature of the carrier escape of the InAs/GaAs QDSC by numerical simulation. The energy band model is illustrated in Fig. 3(a). By assuming identical or separate time constants for the intersubband carrier transfer processes in the ground and excited states, a device-level model developed in combining drift-diffusion equations for the barrier and rate equations for the QD kinetics was successfully applied.[47,48] Figure 3(b) shows their simulated results. The nonexcitonic cell clearly shows a nearly linear behavior in the short-circuit condition ($J_{\text{Non-excitonic}} \approx J_{\text{Non-excitonic, filtered}} + J_{\text{Reference cell}}$). On the other hand, the excitonic cell exhibits a strong nonlinear operation ($J_{\text{Excitonic}} \neq J_{\text{Excitonic, filtered}} + J_{\text{Reference cell}}$).[49] The linear behavior of the nonexcitonic QDSC indicates that practically all the extra carriers contributed by the QDs are being collected at the cell contacts.[40,42] On the contrary, the nonadditive characteristic shown by the QD current in the excitonic QDSC suggest that all the carriers photogenerated at the QDs are recombining. Further analysis has been performed by visualizing the processes of carrier interchange between states at each QD layer. The results revealed that the increment of the recombination is mainly due to the increased hole population in the QDs while playing a central role in the response of the excitonic device.

The effect of the internal electric field on carrier escape and separation was investigated quantitatively by Kasamatsu et al.[50] They have experimentally fabricated InAs/GaAs QDSC with different built-in electric fields by controlling the thickness of intrinsic buffer layers surrounding the InAs/GaAs QDs. The internal electric fields applied to the QDs were estimated as 46 and 193 kV/cm when the total intrinsic layer thicknesses were 299.3 and 69.8 nm, respectively. The authors calibrated the electric field effect by monitoring the carrier dynamic behavior using time-resolved photoluminescence (PL) measurements.[50] Figure 4 displays the detection wavelength dependence of the PL decay profile measured at 3K. The sample with 46 kV/cm shows a double exponential decay. The rapid initial decay is slightly shorter than 2 ns, and the following slow decay becomes longer than 2 ns. For an extremely large internal electric field as 193 kV/cm, the decay is very fast and can be described by double exponential components of s1 and s2 (s1 < s2).[51] A strong electric field of 193 kV/cm causes tunneling-assisted electron escape that occurs easily. The electron escape rapidly reduces the PL intensity with a time constant s1 of 0.46 ns. This short lifetime in the high electric field will prevent photoexcitation of electrons in the intermediate band (IB) in QDs.[51–53] Meanwhile, as mentioned in Sec. 2.1, the dark saturation current J_0 is treated as radiative recombination based on the detailed balance principle. For the sample with a high internal electric field, the existence of additional tunneling recombination path will increase the dark saturation current J_0, and the V_{oc} of this SC eventually reduces according to Eqs. (2) and (4).[37,50]
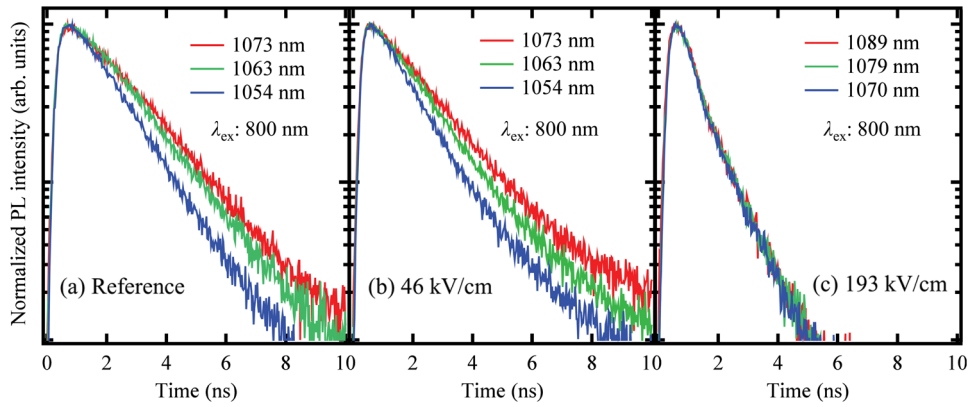
Fig. 4 Detection wavelength dependence of PL decay profile measured at 3 K for (a) a reference sample and SCs at (b) 46 and (c) 193 kV/cm. The excitation laser wavelength was 800 nm, which provides excitation above the GaAs barrier. The excitation powers for (a), (b), and (c) were 100, 100, and 250 μW, respectively. Reprinted with permission from Ref. 50. © 2014 AIP Publishing LLC.

In addition to the internal electric field, the external electric field has also been reported to exert influence on the carrier dynamics. Shiokawa et al.[54] have reported an inplane ultra-high-density InAs (2.2 mL) QDs with density of $3 \sim 5 \times 10^{11}$ cm^{-2} grown on the GaAsSb/GaAs(001) by molecular beam epitaxy. By applying voltage ranging from $+1.0$ V to -1.0 V, the PL decay time showed strong bias dependence, as shown in Fig. 5(a). In particular, the long decay time of 10 ns was obtained at $+1.0$ V.[54] By applying forward bias, it favors the formation of in-plane coupling among the QDs. This is again confirmed in Fig. 5(b) by the PL peak energy shift under different bias voltages. For the forward bias condition, the PL peak shifted toward the low energy side because the enhanced coupling among QDs caused the electron to relax at much lower ground energy states in the QDs with large size.[22,23,55] Meanwhile, the reverse bias was also found to shift the PL peak energy to long wavelength side. This was partially attributed to the strong Stark effect and partially to the fast electron escape rate, which greatly suppressed the high energy interband transition in the QDs.

2.3 Doping Effect on InAs/GaAs Quantum Dot Solar Cell Performance

Typically, QDs grown in the intrinsic region are subjected to high electric field, and carriers are quickly swept away from the nanostructures as soon as they are excited into the bulk
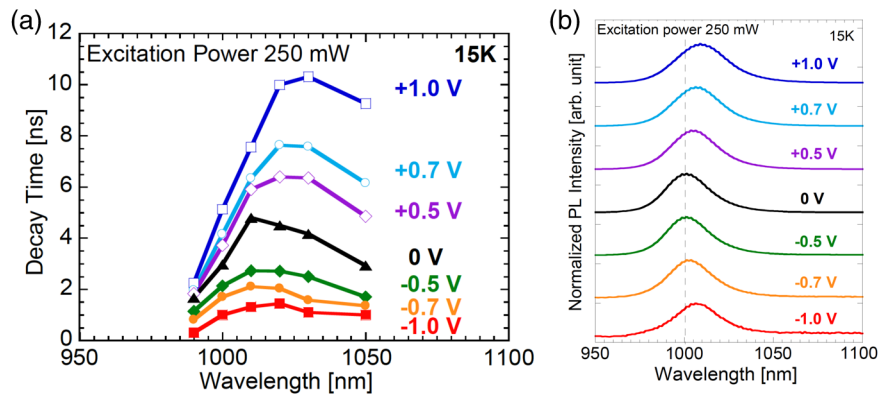

Fig. 5 (a) Relationships between PL decay time spectra and bias voltage. Ultrahigh density InAs QDs with 2.2 mL was inserted into GaAs pn-junction. (b) PL spectra of ultrahigh density InAs QDs with 2.2 mL as a function of bias voltage. Reprinted with permission from Ref. 54. © 2013 IEEE Publishing.
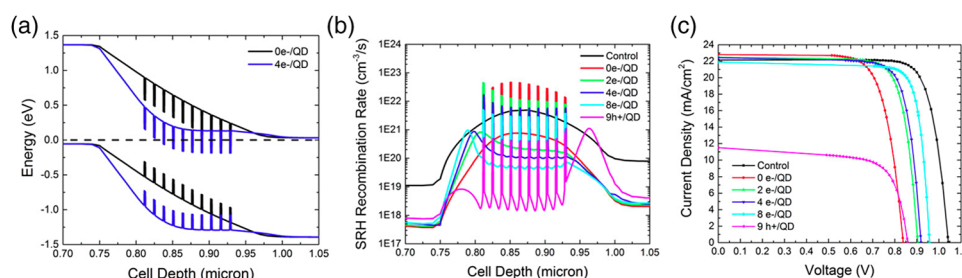
Fig. 6 (a) APSYS modeled band diagram for 0e⁻/QD (black) and 4e⁻/QD (blue) structures in the dark at 0 V applied bias. (b) APSYS modeled SRH rates at 1.0-V applied bias across the i-region of varying delta-doping levels. (c) Measured 1-Sun AM0 $J - V$ characteristics of devices. Reprinted with permission from Ref. 61. © 2014 IEEE Publishing.

continuum.[56–60] Doping QD in the intrinsic region will affect the band profile and, therefore, the electric field in the intrinsic region. Accordingly, the change in electric field will also affect carrier dynamics as well as the solar cell device performance. Polly et al.[61] have reported on both the theoretical and experimental results of the effect of delta-doping in the InAs/GaAs QD on the solar cell performance. Figure 6(a) shows the simulated results where the doping of 4e⁻/QD (e⁻ = electron) has dramatically flattened the i-region and has shifted the intrinsic region to the emitter. A consequence of this shift in the electric field can be seen in Fig. 6(b), which shows the reduced SRH recombination rate at 1.0 V applied bias. They have also found that doping the hole (9h⁺/QD) pushed the intrinsic region toward base layer while reducing the SRH recombination similarly to the electron doping.[47] As shown in Fig. 6(c), the experimental results were consistent with the simulated results. The 8e⁻/QD doping resulted in the highest V_{oc} of 0.932 V, which can be considered a direct effect from the decreased SRH recombination due to the shift of intrinsic region.[29,40] However, the doping-induced band flattening has weakened the carrier collection due to the decreased electric field in the QD region. This negative effect was directly linked to the reduction of J_{sc} for all doped samples. It is interesting to note that the experimental results from Polly et al. are not consistent with the theoretical simulation results by Yoshida et al.[62] The discrepancy is probably because in the simulation an ideal IBSC operation modeling was applied including the electron occupancy in IB, which is usually more difficult to realize by the current doping technique. In other words, the doping in the IB is not able to form the Fermi-level, as shown in the IB region of Fig. 4(b), in the work of Yoshida et al.[62] Therefore, besides the region near the top emitter and the bottom base layer, the occupancy rate in other regions of IB is also not close to the optimal value of 1/2 used in the work of Yoshida et al.

With respect to the doping effect on QDSC, Li et al.[63] have recently reported interesting results regarding electron-doping in QD devices, especially its potential impact on the electron capture potential, which affects (1) carrier collection efficiency and (2) below bandgap photon absorption via transitions to quantum confined states. Figure 7(a) shows the current–voltage characteristics of the fabricated solar cells with different electron doping concentrations. The 0e/dot, 2e/dot to 4e/dot devices exhibit a J_{sc} of 10.1, 11.8, and 12.6 mA/cm², respectively. The authors have interpreted the results as a consequence of so-called "charging" effect. As depicted in Fig. 7(b), when above-bandgap photogenerated electrons move through the QDs layer, the repulsive force exerted by the negatively charged QDs can alter the electron trajectory in such a way as to reduce the probability of electron trapping.[64] The Coulomb potential exerted by the negatively charged QDs is a competing process that acts on the mobile electrons and competes with the QDs trapping potential. When electrons are captured, the trapping effects are progressively deactivated.[65] For the effect (2), the authors found that the 0e/dot device had a much higher external quantum efficiency (EQE) value measured at the QD transition energy (1.1 eV) as compared to the doped QD devices. This was considered a result of the available number of unoccupied confined electron states being reduced with further doping. According to the Fermi's Golden rule, the total transition rate and the absorption in QDs decrease correspondingly, as schematically illustrated in Fig. 7(c).[37,38] These conclusions were further verified by the PL results shown in Fig. 7(d) in which the intensity of QDs emission reduces as the doping increases.
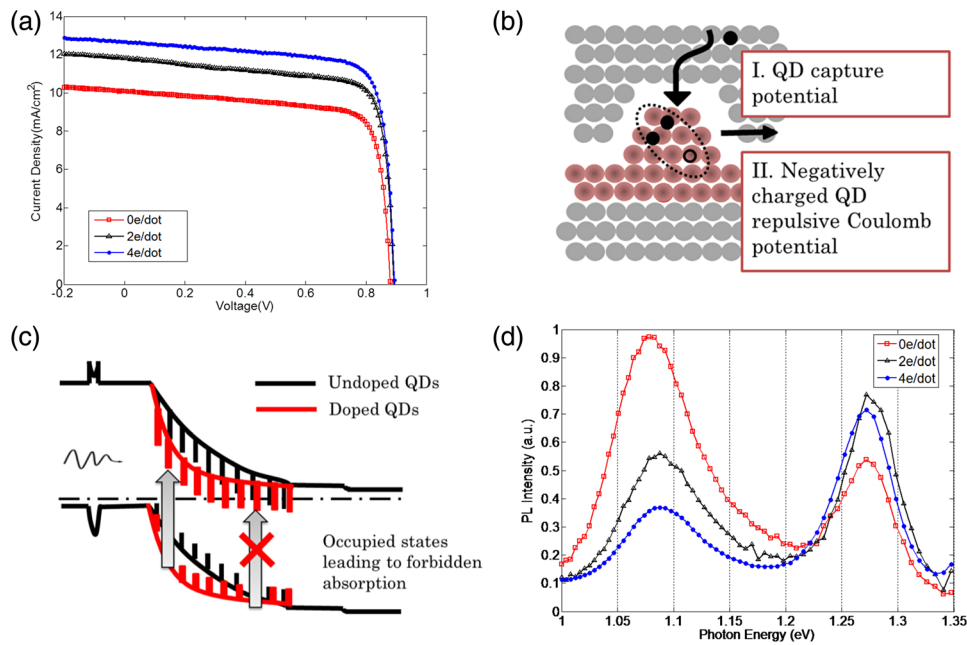
Fig. 7 (a) Current–voltage characteristics of undoped, 2e/dot, and 4e/dot device. (b) Electrons transport through one QD that affected both QD capturing potential and negatively charged excitons repulsive Coulomb potential. (c) Illustration of the effect of band bending on quantum dot states absorption. (d) PL of 0e, 2e, and 4e/dot devices. With further electron-doping, the PL signal at QD ground state (centered at 1.08 eV) reduces while PL signal at wetting layer state (centered at 1.27 eV) enhances. Reprinted with permission from Ref. 63. © 2015 AIP Publishing LLC.

2.4 Effect of Quantum Dot Location on Carrier Transportation and Recombination

QD position in the intrinsic region also showed great influence on carrier dynamics and the device performance.[41,66–68] Driscoll et al.[69] performed simulations on three positions for InAs QD located in the intrinsic region: (1) near the n-doped base, (2) exact center of i-region, and (3) near the p-doped emitter.[69] From the simulation, they found that J_{sc} was nearly identical for the three positions as all were located in a high electric field region and carrier collection remained efficient for all three conditions. However, the model predicts an additional loss of 20 mV in the V_{oc} for the QD located in the exact center of the intrinsic region versus those located near the doped edges.[69] The reduction of the V_{oc} was mainly attributed to SRH recombination, which showed the maximum value when the electron and hole density were similar at the place such as the center of the intrinsic region.[66] They have also fabricated three samples experimentally with the three QD locations mentioned above to verify the simulated results.[69] Figure 8(a) summarized the EQE results for the three samples along with the baseline GaAs cell. It is clear that the bulk spectral response from the QD devices are similar to that of the baseline cell, indicating that neither the introduction of the QDs nor their position has had any adverse effects on the carrier collection efficiency.[69] However, dramatic variation in the V_{oc} was observed, as shown in Fig. 8(b). The emitter-shifted cell exhibited a substantial decrease in V_{oc} down to 0.863 V, as compared to the base-shifted and centered cells with promising voltages of 0.957 and 0.945 V, respectively. The reduction in the emitter-shifted cell was contradictory to the previous theoretical simulation results.[49] A new simulation model was developed by taking the unintentional background n-type doping into consideration, and the reduction of V_{oc} in the emitter-shifted sample was well reproduced and became consistent with the experimental results.

Kechiantz[70] have reported a novel QDSC structure in which a stack of strain-compensated GaSb/GaAs type-II QDs were embedded in the p-doped emitter region, thus spatially far separated from the depletion region. The original motivation for this theoretical work was to find an ultimate solution to the suppression of the reduction of V_{oc} in QD while leaving the advantages of QD intact so that it can still act effectively as additional light absorption source to increase J_{sc},
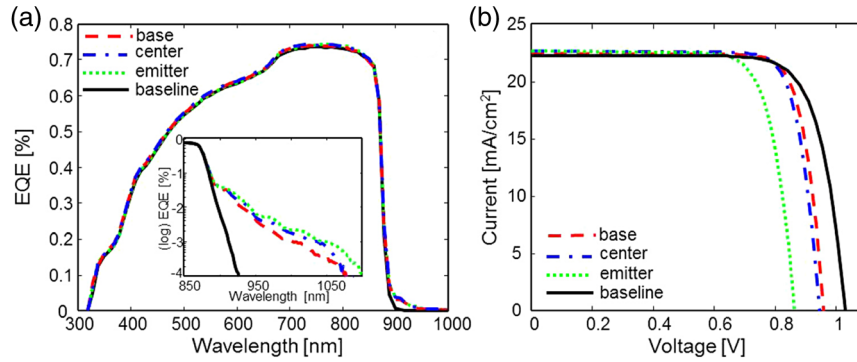
Fig. 8 (a) Measured EQE versus wavelength. (b) Measured current–voltage characteristics for baseline and QD-enhanced pin-GaAs solar cells. The inset highlights the sub-bandgap photoresponse due to absorption by the QD superlattice. Reprinted with permission from Ref. 69. © 2014 AIP Publishing LLC.

as well as the building block for the realizing IBSC with the conservation of V_{oc}.[71,72] The calculation predicts that the concentration from 1-sun to 500-sun increases the efficiency from 30% to 50%, respectively, without the degradation of the V_{oc}.

2.5 Other Featured Carrier Dynamics in InAs/GaAs Quantum Dot Solar Cell

2.5.1 Interdot transportation through Urbach tail

Li et al.[73] have proposed an "extended Urbach tail" model, shown in Fig. 9(a), to explain the interdot carrier transport and below-bandgap photon absorption. They have modeled the Urbach tail with two parameters a_0 and E_1, where E_1 is the characteristic width of the absorption edge and a_0 is a scaling factor.[74] As shown in Fig. 9(b), a fit to the linear dependence up to the edge of the QD transition energy estimated the value for a_0 and E_1 for bulk and QDSC and found 55 meV for QD compared with 15 meV for the bulk GaAs layer.[74] This indicates that an exponentially increasing continuum density of states occurred in the surrounding GaAs matrix, which facilitates the energy relaxation of excited electrons within the QD conduction band potential. The V_{oc} measured for the QDSC is 0.77 V while the bulk GaAs control cell is 0.94 V. The deduced conclusion agrees well with the dark $I - V$ curve fitting analysis results, where they have found that the observed change of lower V_{oc} is due to the change of the SRH recombination coefficient.[37]
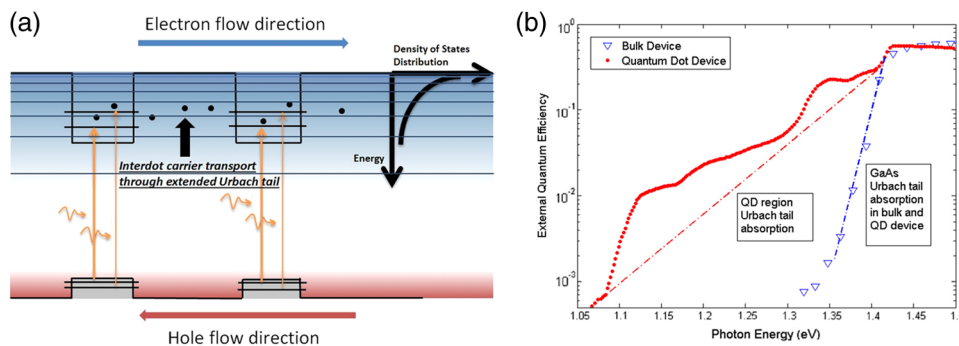

Fig. 9 (a) Schematics of proposed interdot carrier transfer mechanism through continuum density of states due to Urbach tail absorption in the GaAs matrix intrinsic layer and (b) EQE of GaAs/InAs QD sample with no antireflection coating. The Urbach tail contributions for both devices are shown by the dotted lines. Reprinted with permission from Ref. 73. © 2013 AIP Publishing LLC.
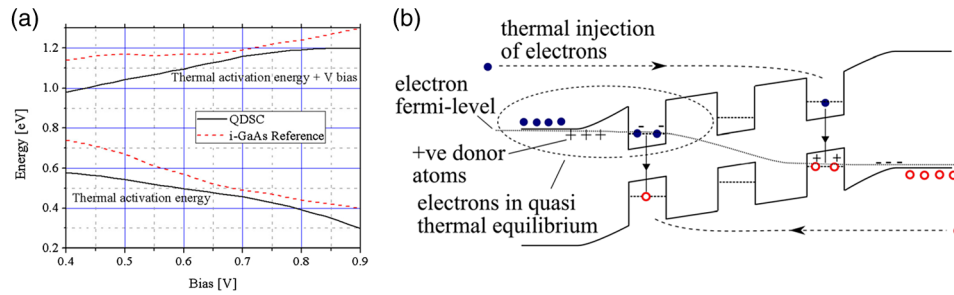
Fig. 10 (a) Dark current activation energy as a function of applied bias as calculated from current values for device temperatures within the 280 to 310 K range. Plots of the activation energy plus the applied bias are also shown. (b) Simplified band diagram of the QDSC. The dominant room temperature dark current mechanisms aredepicted. Reprinted with permission from Ref. 77. © 2000 by John Wiley Sons.

2.5.2 Quantum dot scattering effect on transportation

Semichaevsky and Johnson[75] have used a multiscale model for carrier transport to simulate a p-i-n solar cell that includes InAs/GaAs QDs. Their results suggest that, while contributing to the photocurrent due to absorption of photons with energies less than the bulk GaAs bandgap, stacked layers of InAs QD arrays with high in-plane densities used in a solar cell can inhibit the transport of photocarriers originating from the absorption of photons with energies above bulk GaAs bandgap.[75] Quantum scattering of carriers by the confinement potential, resulting in longer paths travelled by the carriers and thus an increased nonradiative (NR) recombination in the intrinsic region of the cell.[76] The reflected carriers also form an additional space charge that reduces the built-in field in the heterostructure region. As suggested in Eq. (2), an increased NR recombination will cause the reduction of V_{oc}.[37,42,48]

2.5.3 Upper limit of V_{oc} for nearly defect-free InAs/GaAs quantum dot solar cell

One question has recently been raised regarding the realistic upper limit of V_{oc} for InAs/GaAs QDSC. [30,32,34,37,47] Under the ideal case, the device is assumed to be defect-free; therefore, the SRH or NR recombination will be completely eliminated. As discussed in Sec. 2.1, for a InAs/GaAs QDSC to be able to reach the same V_{oc} as GaAs SC, the dark saturation current $J_{0,i+QD}$ must be minimized to the value of $J_{0,i-GaAs}$.[38] Jolley et al.[77] have addressed this issue by performing both experimental and theoretical studies. As shown in Fig. 10(a), a comparison between the InAs/GaAs QDSC and GaAs SC showed that the QDSC has a smaller activation energy of ~0.1 eV than GaAs SC, which is regarded as the leading cause for the reduction of V_{oc}.[78] Figure 10(b) shows the proposed principle in which the QD layer next to the n-layer will have a raised potential, which results in a reduction of the energy required to transport a hole from the p-layer to the QD layers and, therefore, a reduction in dark current activation energy.[79,80] The crucial point to compensate for this 0.1 V reduction in activation energy is that the optical excitation time must be sufficiently short to reduce the carrier occupation in QDs. Given the fast thermal processes, it is expected that intersubband optical excitation time would have to be on the order of 1 ns or below to have a large impact on the dark current processes; this is, however, hardly achievable.[81] Therefore, 0.1 V difference in V_{oc} between InAs/GaAs QDSC and GaAs SC can be regarded as the realistic upper limit for the current InAs/GaAs QDSC and is expected to hold even in the complete absence of crystal defects in the device.

It is noteworthy to mention that in very recent research, Varghese et al.[82] have reported inspiring results by demonstrating a complete voltage recovery in the InAs/GaAs QDSCs by completely suppressing the fast capture of photoelectrons from the GaAs conduction band to the localized states in QDs. The mechanism of this approach reflects exactly the mechanism described in Fig. 10(b), which we proposed for the upper limit of 0.1 V difference.

3 Colloidal Quantum Dot Solar Cells: Interface Engineering for Improving the Photovoltaic Performance

3.1 Introduction

Semiconductor QDs have attracted more and more interest recently because of the following unique properties. First, the energy gaps of the QDs and their absorption spectra can be tuned by changing the size of QDs. Second, QDs have large absorption coefficients resulting from the quantum confinement effect. Third, QDs have a potential to generate multiple electron–hole pairs with one single photon absorption [i.e., the multiple exciton generation (MEG)], which would lead to incident-photon-to-current efficiencies of over 100%. Thus, it has been predicted theoretically that the maximum thermodynamic efficiency for photovoltaic devices could be improved to as much as ~44% by employing semiconductor QDs, which is much higher than the Shockley–Queisser limit (33%).[2–5] QDs can be prepared with chemical methods, which are all called CQDs here to make a difference from the QDs prepared with epitaxial growth method, as mentioned in Chapter 2. The CQDs have the advantages of low-temperature fabrication and solution-based processing, which can make the preparation cost very inexpensive.[24,25] Thus, CQDSCs have been expected to be a candidate of cost-effective next generation solar cells. In recent years, two kinds of CQDSCs—QD-sensitized solar cells (QDSSCs) and quantum dot heterojunction solar cells (QDHSCs)—have been developed rapidly.[24,25] Great efforts have been devoted to a fundamental understanding of QDSSCs and QDHSCs; specifically, interface engineering has been carried out systematically, which leads to a significant improvement in the record PCE of these CQDSCs from <1% to as high as 11.6%.[83–91] The breakthrough in the CQDSCs mostly results from the rapid development of the synthesis technique of high-quality QDs with lower surface trap states and the interface control through various organic and inorganic ligand exchanges on the QDs.[24,25]

In this chapter, we will focus on the interface engineering strategies developed in recent years for improving the efficiencies of QDSSCs and QDHSCs and the mechanism for the improvement of the photovoltaic performance.

3.2 Quantum Dot Sensitized Solar Cells

Figure 11(a) shows the schematic illustration of the working principle and configuration of typical QDSSCs. Similar to dye sensitized solar cell (DSC), QDSSCs consist of a QD sensitized photoelectrode and a counter electrode separated by a liquid electrolyte. In general, wide bandgap metal oxide (TiO_2, ZnO, and SnO_2; in the following TiO_2 is used as an example) nanostructures [such as nanoparticulate, nanorods, nanowires (NWs), nanotubes, and inverse opal] are used as the photoelectrodes in QDSSCs. QDs can be deposited on the photoelectrodes by two kinds of in-situ growth methods, i.e., chemical bath deposition (CBD) and successive
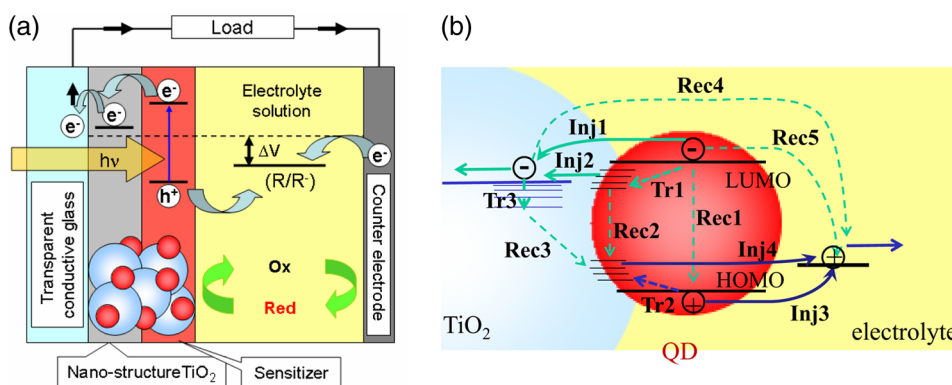

Fig. 11 Schematic illustrations of (a) the working principle and configuration of QD-sensitized solar cells and (b) possible charge transfer processes occurring at TiO_2/QD/electrolyte interfaces, including injection (Inj), trapping (Trp), and recombination (Rec) of photoexcited carriers.

ionic layer absorption and reaction (SILAR), and by adsorption of presynthesized QDs through direct adsorption or linker-assisted QD deposition method.[25,92–94] The *in-situ* deposition methods lead to high loading of QDs, but it is difficult to precisely control the QD size distribution, and surface trap state density in the QDs is high. For the presynthesized QD deposition method, the QDs are size-controlled and high-quality with low surface trap states, but normally the QD loading was low (14%) and thus the PCE was as low as <1%.[95] However, recently, Zhong's group developed a method to increase the QD loading up to 34%, which leads to the highest record PCE of QDSSCs of 11.6%.[87] This is comparable to the record PCE of DSC (11.9%).[91] A number of QDs, such as CdS, CdSe, CdTe, PbS, Sb_2S_3, $CuInS_2$, CdSeTe, $CuInSe_{1-x}S_x$ and core–shell structure or double layered QDs, such as CdSe/CdTe, ZnTe/CdSe, CdS/CdSe, PbS/CdS, have been applied as sensitizers in QDSSCs.[25] Aqueous polysulfide solution is most widely used as the electrolyte for QDSSCs. Some solid-state hole transport materials (HTMs), such as P3HT, Spiro-OMeTAD, and CuSCN, are also used as hole scavenging and transport layers in QDSSCs.[96–98] For the polysulfide electrolyte, copper sulfide (Cu_2S) is the most used counter electrode. For the solid-state HTMs, gold and silver are commonly used as electrodes.

As shown in Fig. 11(a), once electron–hole pairs are generated in the QD sensitizer after optical absorption, photoexcited electrons are injected into the metal oxide electrode and then transported to collection electrode (transparent conducting electrode), while the oxidized QDs are regenerated by electrolyte (hole scavenging medium) and then the oxidized species of redox couple are regenerated at the counter electrode. Figure 11(b) shows the main possible charge transfer processes occurring at TiO_2/QD/electrolyte interfaces, including injection (Inj), trapping (Trp), and recombination (Rec) of both photoexcited electrons and holes.[83] The possible injection paths include electron injection to TiO_2 from LUMO (Inj1) and from electron trapping levels (Inj2) and hole injection to electrolytes from HOMO (Inj3) and from hole trapping levels (Inj4). The possible recombination paths are internal recombination of photoexcited electrons and holes in QDs directly (Rec1) and through trapping levels (Rec2), injected electrons in TiO_2 back transfer to QDs (Rec3, at QD/TiO_2 interface) and to electrolyte (Rec4, at TiO_2/electrolyte interface), recombination of photoexcited electrons in QDs with oxidized species in electrolyte (Rec5, at QD/electrolyte interface).[83] All of the charge transfer processes are key factors for the lower energy conversion efficiency of QDSSCs. In particular, charge recombination at each interface will reduce the charge separation efficiency and charge collection efficiency, which results in poor photovoltaic performance, i.e., low short circuit current J_{sc}, low open circuit voltage V_{oc}, and low fill factor. Here, surface trap states in QDs, which do not exist in molecular dyes of DSCs, are crucial factors for larger recombination and poorer photovoltaic performance in QDSSCs.[94] In the last few years, many strategies, such as (1) surface/interface passivation of QDs and photoelectrodes and (2) use of core–shell QDs or double layered QDs as sensitizers, have been carried out for suppressing the recombination, reducing trapping and improving the injection of electron and holes in the QDSSCs. In the following, an overview of these strategies will be shown.

3.2.1 *Surface passivation*

One important strategy for reducing charge recombination, and thus enhancing charge separation and collection efficiency, is surface passivation on QD-adsorbed photoelectrodes using wide band gap semiconducting materials, such as ZnS, MgO, SiO_2 and Al_2O_3 through post-treatment.[99–104] ZnS deposition with SILAR method was first applied to PbS/CdS cosensitized QDSC,[99] and it has attracted much attention since it was proven to double the PCE of CdSe QDSSCs by Toyoda's group.[100,101] Nowadays, ZnS passivation has become a routine surface passivation method for various QDSSCs, such as CdSe/CdS, and Mn-doped $CuInS_2$, and the PCE of the QDSSCs has been improved largely.[105,106] For example, a PCE as high as 8.1% was reported for CuInSe QDSSCs with ZnS surface passivation.[107] The effects of the ZnS surface passivation and the mechanism for improving the photovoltaic performance of QDSSCs were studied systematically and deeply.[108–110] Hachiya et al.[109] studied the influences of ZnS passivation on charge transfer and recombination dynamics of QDSSCs, such as PbS QDSSCs using transient grating (TG) technique. Their results demonstrate that the ZnS passivation can enhance the charge injection efficiency largely because of the reduction of carrier
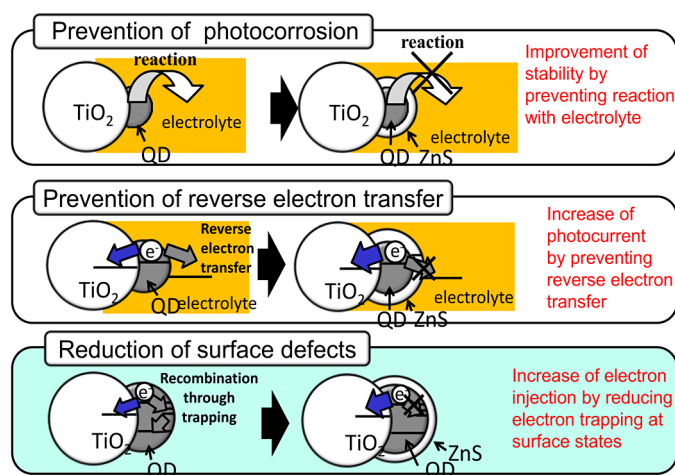
Fig. 12 Schematic illustration of the effects of surface passivation on QD adsorbed photoelectrodes in QD sensitized solar cells: (1) prevention of photocorrosion; (2) prevention of reverse electron transfer; and (3) reduction of surface trap states.

trapping and recombination in PbS QDs after ZnS surface passivation. The ZnS surface passivation was found to play important roles on the stability and the photovoltaic performance of the QDSSCs, as illustrated in Fig. 12: (1) preventing photocorrosion of QDs in electrolyte and improving the stability; (2) preventing reverse electron transfer from TiO_2 to electrolyte and increasing charge collection efficiency; and (3) reducing surface trap states of QDs and thus increasing electron injection efficiency.

ZnSe was used as surface passivation material instead of ZnS for some QDSSCs, such as CdS, CdSe, and CuInS$_2$ QDSSCs.[111–114] Tachan et al.[102] applied MgO to QDSSCs as surface passivation layer.[102] MgO was deposited on TiO_2 electrode before and after QD adsorption, and it was found that charge recombination can be reduced significantly because of MgO surface passivation. Surface modification of QDSSCs with SiO_2 coating resulted in enhanced photovoltaic performance due to suppression of back electron transfer from the photoelectrode to electrolyte.[103] Al_2O_3 is also a useful material for the passivation of QDSSCs and was demonstrated to decrease charge recombination and enhance electron lifetime in solid-state CdS QDSSCs.[104] As discussed earlier for ZnS coating, these wide bandgap semiconductor coating layers act as energy barriers to prevent the photoexcited electrons in QDs and TiO_2 from recombination with oxidized species in electrolyte or solid-state HTMs.

Recently, Zhong's group made a great development in the surface passivation technique, and the PCE of QDSSCs has been enhanced step by step; now, a certified PCE of over 11% has been achieved.[25,86,87] First, they employed a unique double barrier ZnS/SiO_2 coating on the QD adsorbed photoelectrodes.[115] As a result, the PCE of CdSe$_x$Te$_{1-x}$ QDSSCs was improved from 6.37% to 8.55% (certified PCE of 8.21%). They found that the double-layer ZnS/SiO_2 surface passivation could significantly reduce electron dissipation at the outermost surface of photoelectrodes and electron back recombination and largely increase the charge collection efficiency and device stability.[115] Then, they further improved the double layer passivation method by inserting an amorphous TiO_2 (a-TiO_2) layer between the photoelectrode and ZnS/SiO_2 passivation layer (Fig. 13), by which method the PCE of CdSe$_x$Te$_{1-x}$ QDSSCs was increased to 9.28% (certified PCE of 9.01%).[116] They also investigated a series of metal oxyhydroxide coating on photoelectrode in QDSSCs and found that NbCl and ZrO_2Cl_2 modification can improve the photovoltaic properties, especially the open-circuit voltage, and a best PCE of 9.73% was obtained for CdSe$_x$Te$_{1-x}$ QDSSCs.[117]

Very recently, an impressive PCE of 11.6% was reported for Zn-Cu-In-Se QDSSCs with the ZnS/SiO_2 surface passivation, which is the best certified efficiency of QDSSCs up until now.[87] Besides the inorganic material passivation, organic agent passivation, such as dimethylamine, ethylenediamine, ethanedithiol (EDT), thioglycolic acid, and formic acid, were also applied to
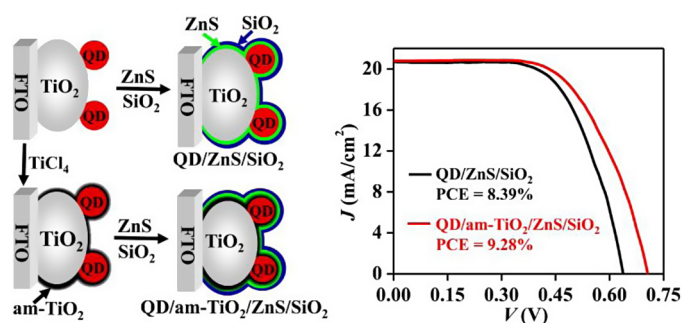
Fig. 13 An improved surface passivation on photoelectrode with an amorphous TiO_2 (am-TiO_2)/ZnS/SiO_2 and the PCE of $CdSe_xTe_{1-x}$ QDSSCs was improved to 9.28%. Reprinted with permission from Ref. 116. © 2015, American Chemical Society.

QDSSCs by Barea et al.[118] and de la Fuente et al.[119] In addition, double passivation with inorganic ZnS and the above organic agents were employed on QDSSCs, and it was found that the inorganic/organic multilayer surface passivation can suppress the recombination more completely and can improve the PCE of QDSSCs further.

By applying various surface passivation on the QDSSCs as mentioned above, the surface trap states of the QDs were reduced greatly and the reverse electron transfer from the QD-sensitized photoelectrodes to electrolyte was prevented effectively. Thus, the PCEs increased dramatically, as summarized in Table 1. On the other hand, the passivation coating also works as a barrier for the photoexcited holes in the QDs. Therefore, the thickness of the passivation coating is also very crucial and the holes excited in the QDs cannot transfer effectively to hole transfer materials, such as the electrolyte if the thickness of the passivation coating is too large. It has been confirmed that there are optimized thicknesses or coating times for the surface passivation of the QDSSCs.[109]

Table 1 Some recent advances in QDSSCs discussed in the paper.

Type of QDSC	Device parameter	PCE	References
CdSe QDSSCs	ZnS passivation	2.1%	100, 101
CdS/CdSe QDSSCs	ZnS passivation	4.92%	105
Mn-doped $CuInS_2$	ZnS passivation	5.38%	106
CuInSe QDSSCs	ZnS passivation	8.1%	107
$CdSe_xTe_{1-x}$ QDSSCs	ZnS/SiO_2 passivation	8.55%	115
$CdSe_xTe_{1-x}$ QDSSCs	a-TiO_2/ZnS/SiO_2 passivation	9.28%	116
$CdSe_xTe_{1-x}$ QDSSCs	NbCl and ZrO_2Cl_2 modification	9.73%	117
Zn-Cu-In-Se QDSSCs	ZnS/SiO_2 passivation	11.6%	87
PbS/CdS QDSSCs	ZnS passivation	4.2%	124
PbS/CdS QDSSCs	ZnS/SiO_2 passivation	7.19%	128
CuInS2/ZnS QDSSCs	ZnS passivation	7.04%	129
CdTe/CdSe QDSSCs	ZnS passivation	6.76%	130
ZnTe/CdSe QDSSCs	ZnS passivation	6.82%	131
CdTe/CdS/CdS QDSSCs	CdS passivation	6.32%	132
CdS/CdSe QDSSCs	ZnS passivation	5.32%	134

3.2.2 *Double-layered quantum dots and core/shell structured quantum dots sensitization*

Double-layered QDSSCs, such as CdS/CdSe and PbS/CdS, have been demonstrated to show better photovoltaic performances than the single-layer QDSSCs, such as CdSe and PbS QDSSCs.[105,120–125] CdS/CdSe QDSSCs was first reported by Niitsoo et al.[120] Then, Lee and Lo[121] clarified that the band position alignment occurred and CdSe band position shifted upward when CdS was deposited between TiO_2 and CdSe, which results in smooth electron transfer from the QDs to TiO_2. Zhang et al.[105] reported a PCE of 4.9% by optimizing the TiO_2 photo-electrode nanostructure. Recently, Osada et al.[123] confirmed that the PCE was enhanced by 70% if CdS was adsorbed on TiO_2 before CdSe adsorption, but the PCE was lowered by 50% if CdS was adsorbed after CdSe adsorption.[123] They studied the mechanism by measuring the charge dynamics using transient absorption and TG methods, and they clarified that the photoexcited electrons could be injected to TiO_2 smoothly due to the cascade band edge alignment of CdSe/CdS/TiO_2. PbS/CdS double-layered QDSSCs together with the control PbS QDSSCs were studied by several groups.[124,125] It was observed clearly that the outer layer of CdS could improve the photocurrent and, thus, the PCE of the QDSSCs largely.[124] It was clarified that the electron trapping and recombination could be suppressed effectively, which resulted in a significant increase in the electron injection efficiency by the CdS passivation on PbS-sensitized photoelectrode.[125]

On the other hand, presynthesized core/shell structured QDs, where an epitaxial surface layer of a different material is grown around the core QD, have been proven to be useful sensitizers for the inhibition of charge recombination in QDSSCs. The core–shell structured QDs are divided into different types: type I, type II, and inverted type I, according to the relative energy band positions of the core and shell semiconductor materials, as shown in Fig. 14.[25] For type I core/shell structured QDs, the shell material has higher CB edge and lower VB edge than those of core material, as shown in Fig. 14(a). The shell reduces the trap state density of the core surface remarkably and works as an energy barrier for photoexcited electrons at the QD/electrolyte interface. Thus, the electron back transfers from the core to electrolyte and from TiO_2 to the trap states of QDs, as well as recombination with the holes in the core, can be largely suppressed. However, the shell thickness has to be thin enough (<1 nm) to ensure that the photoexcited electrons and holes can be injected from the core to the photoelectrode and electrolyte, respectively, by tunneling through the shell.[126] Lai et al.[127] reported direct deposition of PbS/CdS core/shell QDs on mesoporous TiO_2 electrode, and a PCE of 1.28% was obtained. Very recently, Jiao et al.[128] studied the shell thickness dependence of photovoltaic performance of PbS/CdS core/shell QDSSCs. The QDs were deposited on the TiO_2 mesoporous electrode using the capping ligand-induced self-assembly method, and ZnS/SiO_2 passivation was carried out. They found that photoexcited carrier lifetimes in the QDs, electron injection efficiency from the core to TiO_2, and charge recombination depended greatly on the shell thickness. A maximum PCE as high as 7.19% was achieved when the shell thickness was 0.33 nm.[128] Another example is type I $CuInS_2$ (CIS)/ZnS core/shell QDSSCs reported by Pan et al.[129] The ZnS thin layer significantly reduced the surface trap state density of CIS core and charge recombination. As a result, a certified PCE of 7.04% was achieved for an optimized thickness of ZnS shell.
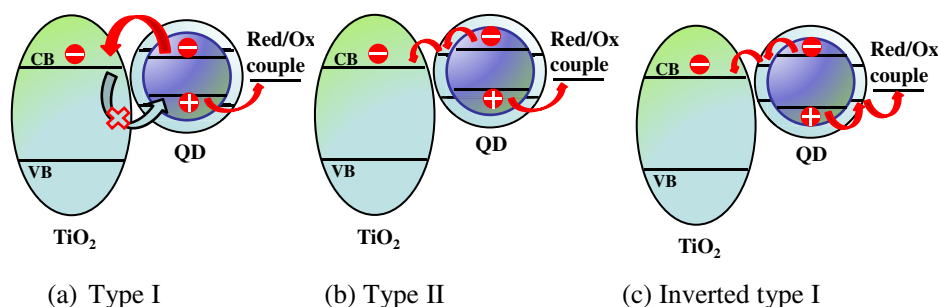

(a) Type I   (b) Type II   (c) Inverted type I

Fig. 14 Schematic illustration of the structures of core/shell QDs: (a) type I, (b) type II, and (c) inverted type I.
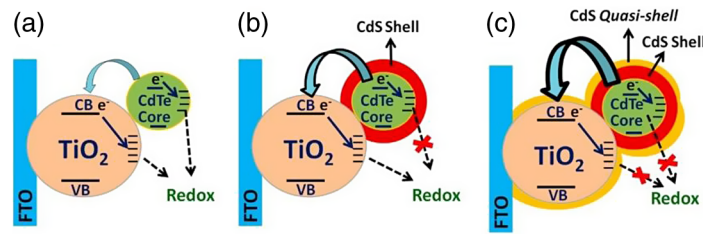
Fig. 15 Schematic illustration of the band diagram of the core/shell/quasishell QDSSCs: (a) CdTe core, (b) CdTe/CdS core/shell, and (c) CdTe/CdS/CdS core/shell/quasishell QDSSCs, respectively. Reprinted with permission from Ref. 132. © 2015, American Chemical Society.

In type II core/shell QDs, both conduction and valence bands of the core material are either higher or lower than those of the shell material [Fig. 14(b)]. If the valence and conduction bands of the shell are both lower, the photoexcited electrons are confined in the shell and the holes are confined in the core. Thus, the electrons and holes are spatially separated from each other, which results in an exciplex state absorption (a red-shift of the absorption edge) and longer lifetime of the photoexcited carriers. Up until now, several kinds of type II core/shell QDs, such as ZnSe/CdS, ZnTe/ZnSe, CdTe/CdSe and ZnTe/CdSe, have been applied as sensitizers.[25,130–132] Recently, CdTe/CdSe core/shell QDSSCs were demonstrated to show larger electron injection efficiency and minimized charge recombination rate, resulting in a PCE of 6.76%.[130] ZnTe/CdSe core/shell QDSSCs showed a faster electron injection rate compared to that of CdTe/CdSe QDs because of the larger conduction band offset, and a certified PCE of 6.82% was achieved.[131] A unique CdTe/CdS (epitaxial)/CdS (nonepitaxial) core/shell/quasi-shell QDSSCs were reported by Sahasrabudhe and Bhattacharyya.[132] They observed that the epitaxial shell passivates the core surface traps and the nonepitaxial quasishell passivates the TiO_2 surface states, as shown in Fig. 15. As a result, a PCE of 6.32% was obtained, which was higher than that of the CdTe/CdS core/shell QDSSCs.

For inverted type-I core/shell structured QDs, the shell material has a narrower band gap compared to the core material and is epitaxially grown around the core [Fig. 14(c)]. Then, a cascade band edge alignment is produced, so photoexcited electrons and holes will transfer to the shell from the core and they will transfer to TiO_2 and electrolyte easily. An inverted type I CdS/CdSe core/shell QD-sensitized solar cell was reported and a PCE of 5.32% was obtained.[133]

Besides the above mentioned type I, type II, and inverted type I core/shell QDs, there is a kind of gradient alloyed QDs in which the element transition is not abrupt in the QDs.[134] Kim et al.[133] reported a simple hot injection method to synthesize the colloidal $CuInTe_{2-x}Se_x$ gradient alloyed QDs with the highest selenium content at the surface of the applications to solar cells. The solution-processed solar cell based on the gradient alloyed $Cu_{0.23}In_{0.36}Te_{0.19}Se_{0.22}$ QDs was prepared, and a PCE of 3.1% was achieved. It was found that the gradient alloyed $Cu_{0.23}In_{0.36}Te_{0.19}Se_{0.22}$ QDs exhibited greatly improved stability over the $CuIn_{1.5}Te_{2.5}$ QDs.

3.3 Quantum Dot Heterojunction Solar Cells

There are two typical architectures of QDHSCs: planar depleted heterojunction and bulk HQDSCs.[24,135] Figure 16 shows examples of the device structures and the working principles of these two kinds of QDHSCs.[135] Typical planar depleted HSC is basically composed of a transparent conduction electrode (ITO or FTO), a metal oxide semiconductor thin layer with a thickness of a few 10 nm, an absorbing QD film with a thickness from a few 10 nm to a few 100 nm, and a metal electrode such as Au. The QDs are presynthesized and dispersed in solution with surface passivation of oleic acid (OA) and spin coated on the metal oxide substrate. The QD surface ligand exchange from the original long organic ligand OA to a short organic ligand or inorganic molecule is very crucial for improving the carrier mobility and diffusion length of the QD film and minimizing the possible surface trap states induced during the ligand exahnge.[24,136] Nowadays, the picture of the working principle of the planar QDHSCs is considered as follows [Fig. 16(b)].[24,135] The QDs are separated with each other and,
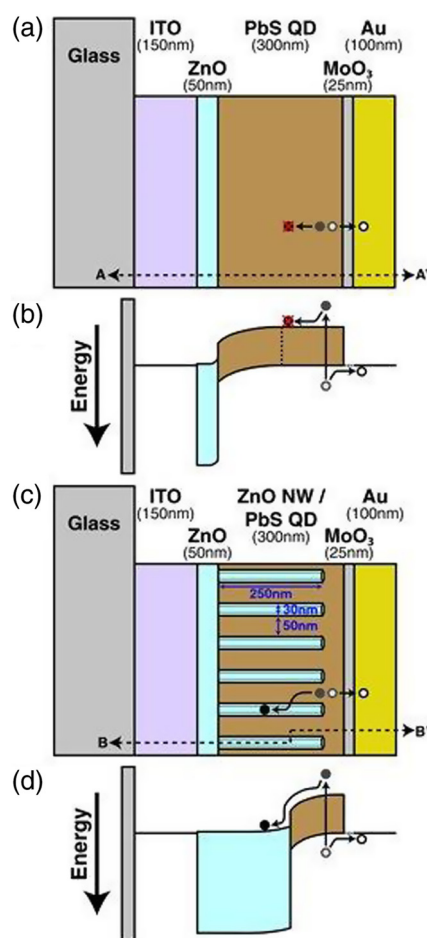
Fig. 16 (a) Schematic and (b) energy band diagram at short-circuit (cross-section along A-A′) of a planar depleted heterojunction QDHSC, and (c) schematic and (d) energy band diagram (cross-section along B-B′) of a bulk heterojunction QDHSC. Reprinted with permission from Ref. 135. © 2013 by John Wiley Sons.

thus, the quantum confinement feature of carriers in QDs is kept. But QD–QD spacing is controlled to be small enough through the ligand exchanging, and, thus, carriers can transfer from one QD to other QDs and move within the QD film through hopping or tunneling. Under working condition of the solar cell, the light is incident from the side of metal oxide semiconductor and absorbed by the QD film. It is believed that a depleted region exists at the heterojunction of metal oxide/QDs and a quasineutral region exists near the metal electrode. The photoexcited electrons and holes in the QDs are drifted by the intrinsic electric field existing in the depleted region and diffuse in the quasineutral region to their collection electrodes, respectively. Subsequently, only photoexcited carriers in the depleted region plus the diffusion length can be effectively collected.[24,135] As a result, the thickness of the QD film, and thus the optical absorption, is limited by the sum of the depletion length and the diffusion length. The depletion width depends on the free-carrier density at each side of the junction, especially that of the QD film. The carrier diffusion length is strongly dependent on surface trapping density and the surface passivation ligands of the QDs. For example, the carrier diffusion length is about 100 nm for PbS QD film, and the typical optimum thickness is about 300 nm for planar depleted heterojunction PbS QDSCs. This thickness is not sufficient for absorbing all incident above bandgap solar radiation. One key issue for this type of QDHSCs is to improve the J_{sc}, which is limited by the insufficient thickness of QD film. By contrast, the J_{sc} can be enhanced remarkably in the bulk HQDSCs [Fig. 16(c)],[135] in which nanostructured metal oxides, such as pillars[137] or NW arrays,[135,138–143] are applied and CQDs are interpenetrated into these nanostructured metal oxide. Such a bulk junction structure allows for the extension of the

depletion region as long as micrometers, which results in a great enhancement in optical absorption, charge separation, and collection efficiency simultaneously.[135,138–143] J_{sc} higher than 30 mA/cm^2 has been obtained by this strategy.[138,139] However, the increase of the interfacial area between the metal oxide nanostructure and the QDs results in an increase in interfacial recombination, so the V_{oc} is lower compared to that of planar HQDSCs.[138–140] The morphology and the thickness of the nanostructures of the metal oxide have been demonstrated to be key factors for photovoltaic performances of the bulk HQDSCs.[138,139]

The planar depleted HQDSCs with n-type ZnO and p-type PbSe QDs were first reported by Leschkies et al.,[143] and a PCE of 1.6% was obtained. Then, Luther et al.[88] reported ZnO/PbS QDHSCs with a certified PCE of 3%. The bulk HQDSCs with ZnO NWs and PbSe QDs were also first demonstrated by Leschkies et al.[144] with a PCE of 2%. The main reason for the poor photovoltaic performance of the QDHSCs, especially the low V_{oc}, is the interfacial recombination. During the last few years, the photovoltaic properties of the two kinds of QDHSCs have been improved rapidly due to the advances of the QD preparation method and device engineering.[24,25] In particular, some strategies of interface engineering have been explored to reduce the recombination occurring at (1) the QD surface and/or QD–QD interface;[145–149] (2) the QD/metal electrode (usually Au) interface;[150–152] and (3) the QD/metal oxide (ZnO or TiO$_2$) interface.[139,153,154]

For suppressing the recombination (1), QD surface passivation through organic dithiol ligand[145] and inorganic atomic halide ligand[146] exchanging has been proven to be very useful. In addition, a hybrid organic-inorganic ligand approach could effectively decrease the midgap electronic trap state density of QDs, and an increase in V_{oc} was achieved.[147] Another approach to reduce the midgap trap state density is to passivate the QD surfaces during the synthesis process. Using this method, Zhang et al.[148] achieved high-performance PbSe QDHSCs with record PCE over 6% by using the Cd and Cl passivation. Recently, the same group prepared air stable PbSe QDHSCs (over 50 days) with a certified PCE of 5.9% by passivating the PbSe QD surfaces with halide anions and residual Zn cations through cation-exchange reaction of ZnSe QDs with PbX$_2$ (X = Cl, Br, or I) precursors.[149]

For suppressing the recombination (2) at the QDs/metal electrode interface (i.e., electron transfer from QDs to metal electrode), a strategy of band alignment at the interface was proposed. Brown et al.[150] have demonstrated that the absolute energy level of QD film is critically dependent on surface chemistry and can be modified through ligand exchange. Bawendi et al. introduced an EDT-capped PbS QD layer between an tetrabutylammonium iodide (TBAI)-treated (i.e., iodine passivated) PbS QD layer and the metal electrode to control the band alignment of the QD layers in ZnO/PbS QDHSCs, as shown in Fig. 17. This band alignment engineering led to a certified PCE of 8.55% and the device showed a long-term air stability.[151] Very recently, Cao et al.[152] used the same device structure of ZnO/PbS QDHSCs but replaced TBAI with 1-ethyl-3-methylimidazolium iodide for halide-based ligand exchange, and they achieved a certified PCE of 8.7% and a better long-term photostability was demonstrated.
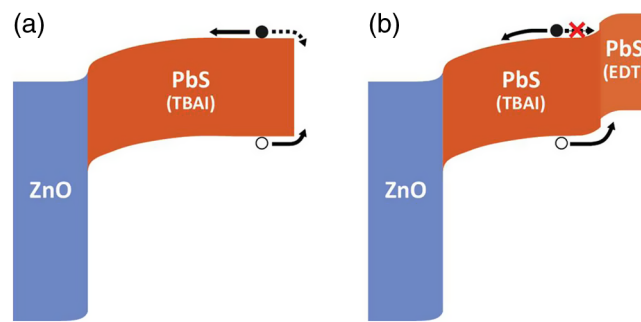

Fig. 17 Schematic illustration of the proposed band bending at short-circuit conditions in the (a) ZnO/PbS–TBAI and (b) ZnO/PbS–TBAI/PbS–EDT (TBAI = tetrabutylammonium iodide). Reprinted with permission from Ref. 151. © 2014 Nature Publishing Group.
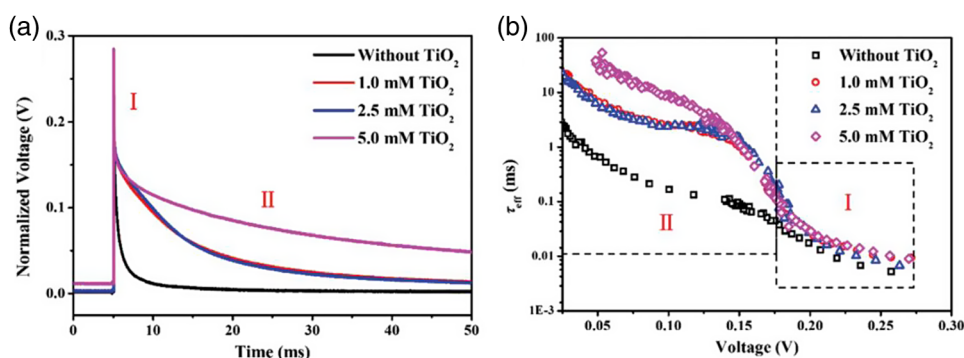
Fig. 18 (a) Normalized open-circuit photovoltage decay curves for bulk heterojunction ZnO/PbS QDHSCs with and without the TiO$_2$ coating on the ZnO-NWs, showing two dominant decay processes, I and II. (b) The effective carrier lifetime calculated from the voltage decay curves.[139]

For suppressing the recombination (3) occurring at the QD/metal oxide interface, surface passivation of the metal oxide nanostructure is very important, especially for bulk HQDSCs. Chang et al.[139] have demonstrated that surface trap state density of ZnO NWs can be reduced greatly by coating a thin TiO$_2$ layer on ZnO NWs in ZnO NW/PbS bulk HSCs. Both transient photovoltage decay and impedance spectroscopy characterizations indicated that the interfacial recombination between PbS and ZnO NWs had been significantly suppressed by the surface passivation strategy. As a result, V_{oc} and PCE have been improved over 40%, and a PCE as high as 6.13% was achieved (device active area: 16 mm^2).[139] It is worth noting that from the transient photovoltage decay, the authors observed that over 40% of the photoexcited carriers had a much faster recombination, as shown in Fig. 18 (recombination I). The authors found that the slower recombination process II became much slower after the TiO$_2$ surface passivation on ZnO NWs, but the faster recombination process I was not influenced by the surface passivation; further, recombination process I was believed to be recombination occurring at QD–QD interface and/or QD/Au interface. Therefore, appropriate passivation of these interfaces can improve the photovoltaic performance further.[139] Jang et al. effectively reduced the interband trap sites of the ZnO nanoparticles by using simple EDT treatment, which resulted in a great suppression of the interfacial recombination in ZnO/PbS QDHSCs. As a result, a certified PCE of 10.14 was achieved.[153] Kim et al.[154] reported a high performance ZnO/PbS QDHSCs with a certified PCE of 10.7% by depositing robust self-assembled monolayers on ZnO surface to adjust the energy alignment of the interface. This is the highest PCE of QDHSCs at the end of 2015. Very recently, the group has achieved a certified PCE of QDHSCs as high as 11.3%.[91] Some recent advances in QDHSCs discussed in the paper is summarized in Table 2.

To push the PCE of QDSCs to be as high as over 40%, as expected theoretically, fundamental studies on MEG in QDs and its realization in practical QDSC devices are very important and have attracted much interest. The MEG has been observed optically in several kinds of QDs, such as PbS, PbSe, PbTe, CdSe, InAs, Si, carbon nanotube, and Cd$_x$Hg$_{1-x}$Te.[155–160] It was found that the generation of multiple-exciton state by MEG in the QDs, such as PbS and PbSe, occurred as fast as a few 100 fs and the relaxation to a single-exciton states on a time scale of a few 10 to a few 100 ps through an Auger like process.[155,159] The extraction of more than one electron per absorbed photon as electrical current in CQDHSCs has been reported with the internal and EQE exceeding 100%, such as PbS, PbSe, and CuInSe$_2$ QDHSCs.[161–163]

For improving the efficiencies of both QDSCs and QDHSCs, photoexcited electron and hole transfer from the QDs are essential, especially for designing the devices of MEG-type QDSCs. Dependence of electron transfer from photoexcited QDs to molecular acceptors on the QD sizes has been studied systematically by Zhu et al.[164] They found that the photoexcited electron transfer rate increased as the QD size decreased, i.e., the driving force increased. The unusual driving force dependence was explained by an Auger-assisted electron transfer model in which the electron transfer could be coupled to the excitation of the hole, circumventing the unfavorable Franck–Condon overlap in the Marcus inverted regime.[164] Olshansky[165] investigated the relationship between driving force and rate for hole transfer from photoexcited QDs systematically

Table 2 Some recent advances in QDHSCs discussed in the paper.

Type of QDSCs	Heterojunction structure	PCE	References
PbSe/ZnO	Planar	1.6%	143
PbSe/ZnO	Planar	3%	88
PbS/ZnO NW	Bulk	4.3%	135
PbS/TiO$_2$ nanopillar	Bulk	5.6%	137
PbS/ZnO NW	Bulk	6.0%	138
PbS/ZnO/TiO$_2$ NW	Bulk	6.13%	139
PbS/TiO$_2$	Planar	6.0%	146
PbS/TiO$_2$	Planar	7.0%	147
PbSe/TiO$_2$	Planar	6.2%	148
PbSe/TiO$_2$	Planar	6.5%	149
PbS/ZnO	Planar	8.55%	151
PbS/ZnO	Planar	8.7%	152
PbS/ZnO	Planar	10.14%	153
PbS/ZnO	Planar	10.7%	154

by using CdSe/CdS core/shell QDs and different molecular hole acceptors. The experimental relationship between the rate and energetic driving force for hole transfer was not well explained by the standard two-state Marcus model because the inverted Marcus region was not observed. An Auger-assisted photoexcited hole transfer mechanism was proposed in which experimental results were modeled successfully.[165] These relationships between interfacial charge transfer and energetic driving force are very useful for designing CQDSCs to maximize interfacial charge transfer and minimize energetic losses associated with the driving force.

4 Summary

In Chapter 2, we reviewed recent research regarding the effect of carrier dynamic behavior on the dark recombination current and the V_{oc} in InAs/GaAs QDSC. It has been shown that the carrier escape nature from the InAs QD formed potential was related to a "retrapping process" occurred at the neighboring QDs. This retrapping process will not only cause the reduction of V_{oc} but also hamper the two-step photon absorption process, which is the key step to realize IBSC. Meanwhile, it has revealed that the carrier separation was affected by both internal and external electric fields. Being affected by the internal electric fields, InAs QDSC showed dependence on the QDs location. By adding the QDs near the n-doped base, higher V_{oc} was confirmed than those located at the center and near p-emitter regions. It has been shown that carrier separation was related to the excitonic dynamics of electrons and holes and the excitonic dynamics was considered responsible for the nonadditive behavior of the photocurrent contributed by the QDs in a QDSC. Doping in QD has also shown a dramatic effect on the V_{oc} through either band-flattening induced internal electric field change or "charging effect" induced trapping deactivation and suppression of the recombination transition. Other effects such as the existence of "Urbach tail" below GaAs bandgap and the scattering effect from InAs QDs caused additional SRH recombination and, therefore, the reduction of V_{oc}. At last, for a nearly defect-free InAs/GaAs QDSC, the V_{oc} was verified as about 0.1 V lower than that of GaAs control cell due to the carrier accumulation in the QDs. This 0.1 V difference in V_{oc} was regarded as the upper limit for a realistic InAs/GaAs QDSC unless the intersubband optical excitation time is sufficiently short to be able to reduce the carrier occupation in QDs.

In Chapter 3, we focused on recent progress in CQDSSCs and CQDHSCs. In the last few years, both QDSSCs and QDHSCs have developed rapidly because of great efforts in interface engineering of these CQDSCs. The certified PCEs of both QDSSCs and QDHSCs have reached as high as over 11% through various interface engineering strategies. However, the PCEs are still much lower than the theoretical value of 44%. Therefore, further fundamental studies on the mechanism of how to improve the efficiency of CQDSCs are very necessary and important. The photovoltaic performances of the CQDSCs would be improved further by solving the following issues: (1) deep understanding, precise control, and passivation of the nanointerfaces of CQDSCs and (2) clarifying the mechanism of multiple exciton generation (MEG) in QDs and realization of MEG in CQDSCs.

Acknowledgments

References

1. A. Luque and A. Marti, "Increasing the efficiency of ideal solar cells by photon induced transitions at intermediate levels," *Phys. Rev. Lett.* **78**, 5014–5017 (1997).
2. A. J. Nozik, "Quantum dot solar cells," *Phys. E.* **14**, 115–120 (2002).
3. A. J. Nozik, "Multiple exciton generation in semiconductor quantum dots," *Chem. Phys. Lett.* **457**, 3–11 (2008).
4. R. D. Schaller and V. I. Klimov, "High efficiency carrier multiplication in PbSe nanocrystals: implications for solar energy conversion," *Phys. Rev. Lett.* **92**, 186601 (2004).
5. M. C. Hanna and A. J. Nozik, "Solar conversion efficiency of photovoltaic and photoelectrolysis cells with carrier multiplication absorbers," *J. Appl. Phys.* **100**, 074510 (2006).
6. Y. Okada et al., "Intermediate band solar cells: recent progress and future directions," *Appl. Phys. Rev.* **2**, 021302 (2015).
7. J. Wu et al., "Quantum dot optoelectronic devices: lasers, photodetectors and solar cells," *J. Phys. D: Appl. Phys.* **48**, 363001 (2015).
8. Z. Zheng et al., "Recent progress towards quantum dot solar cells with enhanced optical absorption," *Nanoscale Res. Lett.* **11**, 266 (2016).
9. A. J. Kramer and E. H. Sargent, "The architecture of colloidal quantum dot solar cells: materials to devices," *Chem. Rev.* **114**, 863–882 (2014).
10. J. Duan et al., "Recent advances in critical materials for quantum dot-sensitized solar cells: a review," *J. Mater. Chem. A* **3**, 17497–17510 (2015).
11. X. Wang, "Recent progress in colloidal quantum dot photovoltaics," *Front. Optoelectron.* **8**, 241–251 (2015).
12. K. Sakamoto et al., "Quantum-dot density dependence of power conversion efficiency of intermediate-band solar cells," *J. Appl. Phys.* **112**, 124515 (2012).
13. R. Strandberg and T. W. Reenaas, "Photofilling of intermediate bands," *J. Appl. Phys.* **105**, 124512 (2009).
14. R. Strandberg and T. W. Reenaas, "Drift-diffusion model for intermediate band solar cells including photofilling effects," *Res. Appl.* **19**, 21–32 (2011).
15. R. Oshima, A. Takata, and Y. Okada, "Strain-compensated InAs/GaNAs quantum dots for use in high-efficiency solar cells," *Appl. Phys. Lett.* **93**, 083111 (2008).
16. G. S. Solomon et al., "Vertically aligned and electronically coupled growth induced InAs islands in GaAs," *Phys. Rev. Lett.* **76**, 952–955 (1996).
17. T. Sugaya et al., "Miniband formation in InGaAs quantum dot superlattice," *Appl. Phys. Lett.* **97**, 043112 (2010).
18. Y. Shoji et al., "Effect of spacer layer thickness on multi-stacked InGaAs quantum dots grown on GaAs(311)B substrate for application to intermediate band solar cells," *J. Appl Phys.* **111**, 074305 (2012).

19. D. Alonso-Álvarez et al., "Carrier recombination effects in strain compensated quantum dot stacks embedded in solar cells," *Appl. Phys. Lett.* **93**, 123114 (2008).
20. S. M. Hubbard et al., "Effect of strain compensation on quantum dot enhanced GaAs solar cells," *Appl. Phys. Lett.* **92**, 123512 (2008).
21. F. K. Tutu et al., "Improved performance of multilayer InAs/GaAs quantum-dot solar cells using a high-growth-temperature GaAs spacer layer," *J. Appl. Phys.* **111**, 046101 (2012).
22. E. Saputra et al., "Self-formation of in-plane ultrahigh-density InAs quantum dots on GaAsSb/GaAs(001)," *Appl. Phys. Express* **5**, 125502 (2012).
23. K. Sameshima, T. Sano, and K. Yamaguchi, "Self-formation of ultrahigh-density $(10^{12} \times cm^{-2})$ InAs quantum dots on InAsSb/GaAs(001) and their photoluminescence properties," *Appl. Phys. Express* **9**, 075501 (2016).
24. G. H. Carey et al., "Colloidal quantum dot solar cells," *Chem. Rev.* **115**, 12732–12763 (2015).
25. K. Zhao, Z. Pan, and X. Zhong, "Charge recombination control for high efficiency quantum dot sensitized solar cells," *J. Phys. Chem. Lett.* **7**, 406–417 (2016).
26. C. G. Bailey et al., "Open-circuit voltage improvement of InAs/GaAs quantum-dot solar cells using reduced InAs coverage," *IEEE J. Photovoltaics* **2**, 269–275 (2012).
27. A. Martí, L. Cuadra, and A. Luque, "Quasi-drift diffusion model for the quantum dot intermediate band solar cell," *IEEE Trans. Electron. Dev.* **49**, 1632–1639 (2002).
28. A. S. Lin, W. Wang, and J. Phillips, "Model for intermediate band solar cells incorporating carrier transport and recombination," *J. Appl. Phys.* **105**, 064512 (2009).
29. P. G. Linares et al., "Voltage limitation analysis in strain-balanced InAs/GaAsN quantum dot solar cells applied to the intermediate band concept," *Sol. Energy Mater. Sol. Cells* **132**, 178–182 (2015).
30. A. Datas et al., "Intermediate band solar cell with extreme broadband spectrum quantum efficiency," *Phys. Rev. Lett.* **114**, 157701 (2015)
31. E. López et al., "Demonstration of the operation principles of intermediate band solar cells at room temperature," *Sol. Energy Mater. Sol. Cells* **149**, 15–18 (2015).
32. T. Sogabe et al., "Self-consistent electrical parameter extraction from bias dependent spectral response measurements of III-V multi-junction solar cells," *Prog. Photovoltaics: Res. Appl.* **23**, 37–48 (2015).
33. Y. Shoji, K. Akimoto, and Y. Okada, "Optical properties of multi-stacked InGaAs/GaNAs quantum dot solar cell fabricated on GaAs (311)B substrate," *J. Appl. Phys.* **112**, 064314 (2012).
34. A. Takata et al., "Optical gain of multi-stacked InAs quantum dots grown on InP (311)B substrate by strain-compensation technique," *Phys. Status Solidi (c)* **8**, 254–256 (2011).
35. R. Oshima et al., "High-density quantum dot superlattice for application to high-efficiency solar cells," *Phys. Status Solidi (c)* **8**, 619–621 (2011).
36. T. Sogabe et al., "Enhancement of current collection in epitaxial lift-off InAs/GaAs quantum dot thin film solar cell and concentrated photovoltaic study," *Appl. Phys. Lett.* **105**, 113904 (2014).
37. T. Sogabe et al., "Intermediate-band dynamics of quantum dots solar cell in concentrator photovoltaic modules," *Sci. Rep.* **4**, 4792 (2014).
38. S. Tomić, T. Sogabe, and Y. Okada, "In-plane coupling effect on absorption coefficients of InAs/GaAs quantum dots arrays for intermediate band solar cell," *Prog. Photovoltaics: Res. Appl.* **23**, 546 (2014).
39. T. Sogabe et al., "Theoretical analysis of GaAs/AlGaAs quantum dots in quantum wire array for intermediate band solar cell," *J. Renewable Sustainable Energy* **6**, 011206 (2014).
40. T. Sogabe et al., "Experimental characterization and self-consistent modeling of luminescence coupling effect in III-V multijunction solar cells," *Appl. Phys. Lett.* **103**, 263907 (2013).
41. S. M. Hubbard et al., "Effect of vicinal substrates on the growth and device performance of quantum dot solar cells," *Sol. Energy Mater. Sol. Cells* **108**, 256–262 (2013).
42. D. G Sellers et al., "Analyzing carrier escape mechanisms in InAs/GaAs quantum dot p-i-n junction photovoltaic cells," *Appl. Phys. Lett.* **104**, 223903 (2014).

43. W. M. Reid, T. Driscoll, and M. F. Doty, "Forming delocalized intermediate states with realistic quantum dots," *J. Appl. Phys.* **111**, 056102 (2012).

44. R. Tamaki et al., "Spectrally resolved intraband transitions on two-step photon absorption in InGaAs/GaAs quantum dot solar cell," *Appl. Phys. Lett.* **105**, 073118 (2014).

45. S. Asahi et al., "Saturable two-step photocurrent generation in intermediate-band solar cells including InAs quantum dots embedded in Al0.3Ga0.7 As/GaAs quantum wells," *IEEE J. Photovoltaics* **6**, 465–472 (2016).

46. A. Cedola, F. Cappelluti, and M. Gioannini, "Dependence of quantum dot photocurrent on the carrier escape nature in InAs/GaAs quantum dot solar cells," *Semicond. Sci. Technol.* **31**, 025018 (2016).

47. K. Sablon et al., "Strong enhancement of solar cell efficiency due to quantum dots with built-in charge," *Nano Lett.* **11**, 2311–2317 (2011).

48. D. M. Tex, I. Kamiya, and Y. Kanemitsu, "Efficient upconverted photocurrent through an Auger process in disklike InAs quantum structures for intermediate-band solar cells," *Phys. Rev. B* **87**, 245305 (2013).

49. D. Guimard et al., "Fabrication of InAs/GaAs quantum dot solar cells with enhanced photocurrent and without degradation of open circuit voltage," *Appl. Phys. Lett.* **96**, 203507 (2010).

50. N. Kasamatsu et al., "Effect of internal electric field on InAs/GaAs quantum dot solar cells," *J. Appl. Phys.* **115**, 083510 (2014).

51. C. F. Klingshirn, *Semiconductor Optics*, Springer-Verlag, Berlin, Germany (2007).

52. A. Takahashi et al., "One-dimensional miniband formation in closely stacked InAs/GaAs quantum dots," *Phys. Rev. B* **87**, 235323 (2013).

53. O. Kojima et al., "Photoluminescence characteristics of quantum dots with electronic states interconnected along growth direction," *J. Appl. Phys.* **103**, 113504 (2008).

54. M. Shiokawa et al., "Long carrier lifetime in ultrahigh-density InAs quantum-dot sheet of intermediate band solar cells," in *39th IEEE Photovoltaic Spec. Conf.*, pp. B21–B101 (2013).

55. K. Yamaguchi and T. Kanto, "Self-assembled InAs quantum dots on GaSb/GaAs(001) layers by molecular beam epitaxy," *J. Cryst. Growth* **275**, e2269 (2005).

56. Y. Dai et al., "Investigation of carrier escape mechanism in InAs/GaAs quantum dot solar cells," in *Proc. IEEE 38th Photovoltaic Specialist Conf.*, p. 000039 (2012).

57. A. Alemu and A. Freundlich, "Resonant thermotunneling design for high performance single-junction quantum-well solar cells," *IEEE J. Photovoltaics* **2**, 256–260 (2012).

58. H. J. Hovel and J. M. Woodall, "The effect of depletion region recombination currents on the efficiencies of Si and GaAs solar cells," in *10th IEEE Photovoltaic Specialist Conf.*, pp. 25–30 (1973).

59. K. Driscoll and S. Hubbard, "Modeling the optical and electrical response of nanostructured III-V solar cells," in *Proc. IEEE 38th Photovoltaic Specialist Conf.*, p. 002985 (2012).

60. K. Driscoll et al., "Investigation of the design parameters of quantum dot enhanced III-V solar cells," *Proc. SPIE* **8620**, 86200L (2013).

61. S. J. Polly et al., "Delta-doping effects on quantum-dot solar cells," *IEEE J. Photovoltaics* **4**, 1079–1085 (2014).

62. K. Yoshida, Y. Okada, and N. Sano, "Device simulation of intermediate band solar cells: effects of doping and concentration," *J. Appl. Phys.* **112**, 084510 (2012).

63. T. Li et al., "Enhanced carrier collection efficiency and reduced quantum state absorption by electron doping in self-assembled quantum dot solar cells," *Appl. Phys. Lett.* **106**, 053902 (2015).

64. H. F. Lu et al., "Plasmonic quantum dot solar cells for enhanced infrared response," *Appl. Phys. Lett.* **100**, 103505 (2012).

65. T. Inoue et al., "Impurity doping in self-assembled InAs/GaAs quantum dots by selection of growth steps," *J. Appl. Phys.* **108**, 063524 (2010).

66. J. Nelson et al., "Effect of quantum well location on single quantum well p-i-n photodiode dark currents," *J. Appl. Phys.* **86**, 5898 (1999).

67. T. Morioka and Y. Okada, "Dark current characteristics of InAs/GaNAs strain-compensated quantum dot solar cells," *Phys. E* **44**, 390–393 (2011).

68. J. Nelson, *The Physics of Solar Cells*, Imperial College Press, London, United Kingdom (2003).
69. K. Driscoll et al., "Effect of quantum dot position and background doping on the performance of quantum dot enhanced GaAs solar cells," *Appl. Phys. Lett.* **104**, 023119 (2014).
70. A. Kechiantz, A. Afanasev, and J.-L. Lazzari, "Impact of spatial separation of type-II GaSb quantum dots from the depletion region on the conversion efficiency limit of GaAs solar cells," *Prog. Photovoltaics: Res. Appl.* **23**, 1003–1016 (2015).
71. A. M. Kechiantz, L. M. Kocharyan, and H. M. Kechiyants, "Band alignment and conversion efficiency in Si/Ge type-II quantum dot intermediate band solar cells," *Nanotechnology* **18**, 405401 (2007).
72. S. M. Sze and K. N. Kwok, *Physics of Semiconductor Devices*, Wiley, New York, pp. 40–42 (1981).
73. T. Li, R. E. Bartolo, and M. Dagenais, "Challenges to the concept of an intermediate band in InAs/GaAs quantum dot solar," *Appl. Phys. Lett.* **103**, 141113 (2013).
74. S. R. Johnson and T. Tiedje, "Temperature dependence of the Urbach edge in GaAs," *J. Appl. Phys.* **78**, 5609 (1995).
75. A. V. Semichaevsky and H. T. Johnson, "Carrier transport in a quantum dot solar cell using semiclassical and quantum mechanical models," *Sol. Energy Mater. Sol. Cells* **108**, 189–199 (2013).
76. A.G. Norman et al., "InGaAs/GaAs QD superlattices: MOVPE growth, structural and optical characterization, and application in intermediate-band solar cells," in *31th IEEE Photovoltaic Specialist Conf.*, pp. 43–48 (2005).
77. G. Jolley et al., "The role of intersubband optical transitions on the electrical properties of InGaAs/GaAs quantum dot solar cells," *Prog. Photovoltaics: Res. Appl.* **21**, 736–746 (2013).
78. G. Jolley et al., "Electron-hole recombination properties of In0.5Ga0.5As/GaAs quantum dot solar cells and the influence on the open circuit voltage," *Appl. Phys. Lett.* **97**, 123505 (2010).
79. H. F. Lu et al., "Temperature dependence of dark current properties of InGaAs/GaAs quantum dot solar cells," *Appl. Phys. Lett.* **98**, 183509 (2011).
80. G. Jolley et al., "Properties of $In_{0.5}Ga_{0.5}As/GaAs/Al_{0.2}Ga_{0.8}As$ quantum-dots-in-a-well infrared photodetectors," *J. Phys. D* **42**, 095101 (2009).
81. A. Nozik, "Spectroscopy and hot electron relaxation dynamics in semiconductor quantum wells and quantum dots," *Ann. Rev. Phys. Chem.* **52**, 193–231 (2001).
82. A. Varghese et al., "Complete voltage recovery in quantum dot solar cells due to suppression of electron capture," *Nanoscale* **8**, 7248–7256 (2016).
83. I. Mora-Sero and J. Bisquert, "Breakthroughs in the development of semiconductor-sensitized solar cells," *J. Phys. Chem. Lett.* **1**, 3046–3052 (2010).
84. V. Talapin et al., "Prospects of colloidal nanocrystals for electronic and optoelectronic applications," *Chem. Rev.* **110**, 389–458 (2010).
85. P. V. Kamat, "Quantum dot solar cells," *J. Phys. Chem. Lett.* **4**, 908–918 (2013).
86. J. Yang et al., "CdSeTe/CdS type-I core/shell quantum dot sensitized solar cells with efficiency over 9%," *J. Phys. Chem. C* **119**, 28800–28808 (2015).
87. J. Du et al., "Zn-Cu–In-Se quantum dot solar cells with a certified power conversion efficiency of 11.6%," *J. Am. Chem. Soc.* **138**, 4201–4209 (2016).
88. J. M. Luther et al., "Stability assessment on a 3% bilayer PbS/ZnO quantum dot heterojunction solar cell," *Adv. Mater.* **22**, 3704–3707 (2010).
89. C.-H. M. Chuang et al., "Improved performance and stability in quantum dot solar cells through band alignment engineering," *Nat. Mater.* **13**, 796–801 (2014).
90. G.-H. Kim et al., "High-efficiency colloidal quantum dot photovoltaics via robust self-assembled monolayers," *Nano Lett.* **15**, 7691–7696 (2015).
91. NREL, "File: best research-cell efficiencies.png," Best Research-Cell Efficiencies, https://commons.wikimedia.org/wiki/File:Best_Research-Cell_Efficiencies.png (14 September 2016).
92. C.-H. Chang and Y.-L. Lee, "Chemical bath deposition of CdS quantum dots onto mesoscopic TiO_2 films for application in quantum-dot-sensitized solar cells," *Appl. Phys. Lett.* **91**, 053503 (2007).

93. H. Lee et al., "Efficient CdSe quantum dot-sensitized solar cells prepared by an improved successive ionic layer adsorption and reaction process," *Nano Lett.* **9**, 4221–4227 (2009).

94. G. Hodes, "Comparison of dye- and semiconductor-sensitized porous nanocrystalline liquid junction solar cells," *J. Phys. Chem. C* **112**, 17778–17787 (2008).

95. N. Guijarro et al., "CdSe quantum dot-sensitized TiO$_2$ electrodes: effect of quantum dot coverage and mode of attachment," *J. Phys. Chem. C* **113**, 4208–4214 (2009).

96. Y. Hao et al., "Efficient semiconductor-sensitized solar cells based on poly(3-hexylthio-phene) at CdSe at ZnO core-shell nanorod arrays," *J. Phys. Chem. C* **114**, 8622–8625 (2010).

97. H. S. Kim et al., "High efficiency solid-state sensitized solar cell-based on submicrometer rutile TiO$_2$ nanorod and CH$_3$NH$_3$PbI$_3$ perovskite sensitizer," *Nano Lett.* **13**, 2412–2417 (2013).

98. P. P. Boix et al., "Hole transport and recombination in all-solid Sb2S3-sensitized TiO$_2$ solar cells using CuSCN as hole transporter," *J. Phys. Chem. C* **116**, 1579–1587 (2012).

99. S. Yang et al., "High photostability and quantum yield of nanoporous TiO$_2$ thin film electrodes Co-sensitized with capped sulfides," *J. Mater. Chem.* **12**, 1459–1464 (2002).

100. J. Diguna et al., "High efficiency of CdSe quantum-dot-sensitized TiO$_2$ inverse opal solar cells," *Appl. Phys. Lett.* **91**, 023116 (2007).

101. Q. Shen et al., "Effect of ZnS coating on the photovoltaic properties of CdSe quantum dot sensitized solar cells," *J. Appl. Phys.* **103**, 084304 (2008).

102. Z. Tachan et al., "The importance of the TiO$_2$/quantum dots interface in the recombination processes of quantum dot sensitized solar cells," *Phys. Chem. Chem. Phys.* **15**, 3841–3845 (2013).

103. Z. Liu et al., "Enhancing the performance of quantum dots sensitized solar cell by SiO$_2$ surface coating," *Appl. Phys. Lett.* **96**, 233107 (2010).

104. K. Roelofs et al., "Effect of Al$_2$O$_3$ recombination barrier layers deposited by atomic layer deposition in solid-state CdS quantum dot-Sensitized solar cells," *J. Phys. Chem. C* **117**, 5584–5592 (2013).

105. Q. Zhang et al., "Highly efficient CdS/CdSe-sensitized solar cells controlled by the structural properties of compact porous TiO$_2$ photoelectrodes," *Phys. Chem. Chem. Phys.* **13**, 4659–4667 (2011).

106. J. Luo et al., "Highly efficient core-shell CuInS$_2$-Mn doped CdS quantum dot sensitized solar cells," *Chem. Commun.* **49**, 3881–3883 (2013).

107. J.-Y. Kim et al., "Highly efficient copper indium selenide quantum dot solar cells: suppression of carrier recombination by controlled ZnS overlayers," *ACS Nano* **9**, 11286–11295 (2015).

108. N. Guijarro et al., "Uncovering the role of the ZnS treatment in the performance of quantum dot sensitized solar cells," *Phys. Chem. Chem. Phys.* **13**, 12024–12032 (2011).

109. S. Hachiya et al., "Effect of ZnS coatings on the enhancement of the photovoltaic properties of PbS quantum dot-sensitized solar cells," *J. Appl. Phys.* **111**, 104315 (2012).

110. J. Chang et al., "Uncovering the charge transfer and recombination mechanism in ZnS-coated PbS quantum dot sensitized solar cells," *Sol. Energy* **122**, 307–313 (2015).

111. Z. Ning et al., "Solar cells sensitized with type-II ZnSe-CdS core/shell colloidal quantum dots," *Chem. Commun.* **47**, 1536–1538 (2011).

112. C. Liu et al., "Boosting the cell efficiency of CdSe quantum dot sensitized solar cell via a modified ZnS post-treatment," *Electrochim. Acta* **111**, 179–184 (2013).

113. J. Y. Chang et al., "Efficient 'green' quantum dot-sensitized solar cells based on Cu2S-CuInS2–ZnSe architecture," *Chem. Commun.* **48**, 4848–4850 (2012).

114. A. V. V. M. Gopi et al., "Improved photovoltaic performance and stability of quantum dot sensitized solar cells using Mn-ZnSe shell structure with enhanced light absorption and recombination control," *Nanoscale* **7**, 12552–12563 (2015).

115. K. Zhao et al., "Boosting power conversion efficiencies of quantum-dot-sensitized solar cells beyond 8% by recombination control," *J. Am. Chem. Soc.* **137**, 5602–5609 (2015).

116. Z. Ren et al., "Amorphous TiO$_2$ buffer layer boosts efficiency of quantum dot sensitized solar cells to over 9%," *Chem. Mater.* **27**, 8398–8405 (2015).

117. Z. Ren et al., "Effects of metal oxyhydroxide coatings on photoanode in quantum dot sensitized solar cells," *Chem. Mater.* **28**, 2323–2330 (2016).

118. E. M. Barea et al., "Design of injection and recombination in quantum dot sensitized solar cells," *J. Am. Chem. Soc.* **132**, 6834–6839 (2010).

119. S. de la Fuente et al., "Effect of organic and inorganic passivation in quantum-dot- sensitized solar cells," *J. Phys. Chem. Lett.* **4**, 1519–1525 (2013).

120. O. Niitsoo et al., "Chemical bath deposited CdS/CdSe-sensitized porous TiO₂ solar cells," *J. Photochem. Photobiol. A* **181**, 306–313 (2006).

121. Y.-L. Lee and Y.-S. Lo, "Highly efficient quantum-dot- sensitized solar cell based on Co-sensitization of CdS/ CdSe," *Adv. Funct. Mater.* **19**, 604–609 (2009).

122. T. Toyoda et al., "Photoacoustic and photoelectrochemical current spectra of combined CdS/CdSe quantum dots adsorbed on nanostructured TiO₂ electrodes, together with Photovoltaic Characteristics," *J. Appl. Phys.* **108**, 114304 (2010).

123. N. Osada et al., "Photoexcited carrier dynamics of double-layered CdS/CdSe quantum dot sensitized solar cells measured by heterodyne transient grating and transient absorption methods," *Phys. Chem. Chem. Phys.* **16**, 5774–5778 (2014).

124. V. González-Pedro et al., "High performance PbS quantum dot sensitized solar cells exceeding 4% efficiency: the role of metal precursors in the electron injection and charge separation," *Phys. Chem. Chem. Phys.* **15**, 13835–13843 (2013).

125. K. Sato et al., "The effect of CdS on the charge separation and recombination dynamics in PbS/CdS double-layered quantum dot sensitized solar cells," *Chem. Phys.*, in press (2016). (in press).

126. H. Zhu et al., "Controlling charge separation and recombination rates in CdSe/ZnS type I core-shell quantum dots by shell thicknesses," *J. Am. Chem. Soc.* **132**, 15038–15045 (2010).

127. L. H. Lai et al., "Sensitized solar cells with colloidal PbS-CdS core-shell quantum dots," *Phys. Chem. Chem. Phys.* **16**, 736–742 (2014).

128. S. Jiao et al., "Surface engineering of PbS quantum dot sensitized solar cells with a conversion efficiency exceeding 7%," *J. Mater. Chem. A* **4**, 7214–7221 (2016).

129. Z. Pan et al., "High-efficiency 'green' quantum dot solar cells," *J. Am. Chem. Soc.* **136**, 9203–9210 (2014).

130. J. Wang et al., "Core/shell colloidal quantum dot exciplex states for the development of highly efficient quantum dot sensitized solar cells," *J. Am. Chem. Soc.* **135**, 15913–15922 (2013).

131. S. Jiao et al., "Band engineering in core/shell ZnTe/CdSe for photovoltage and efficiency enhancement in exciplex quantum dot sensitized solar cells," *ACS Nano* **9**, 908–915 (2015).

132. A. Sahasrabudhe and S. Bhattacharyya, "Dual sensitization strategy for high-performance core/shell/quasi-shell quantum dot solar cells," *Chem. Mater.* **27**, 4848–4859 (2015).

133. Z. Pan et al., "Highly efficient inverted type-I CdS/CdSe core/shell structure QD sensitized solar cells," *ACS Nano* **6**, 3982–3991 (2012).

134. S. Kim et al., "Fabrication of CuInTe₂ and CuInTe₂ₓSeₓ ternary gradient quantum dots and their application to solar cells," *ACS Nano* **7**, 4756–4763 (2013).

135. J. Jean et al., "ZnO nanowire arrays for enhanced photocurrent in PbS quantum dot solar cells," *Adv. Mater.* **25**, 2790–2796 (2013).

136. R. Wang et al., "Colloidal qantum dot ligand engineering for high performance solar cells," *Energy Environ. Sci.* **9**, 1130–1143 (2016).

137. A. J. Kramer et al., "Ordered nanopillar structured electrodes for depleted bulk heterojunction colloidal quantum dot solar cells," *Adv. Mater.* **24**, 2315–2319 (2012).

138. H. Wang et al., "PbS-quantum-dot-based heterojunction solar cells utilizing ZnO nanowires for high external quantum efficiency in the near-infrared region," *J. Phys. Chem. Lett.* **4**, 2455–2460 (2013).

139. J. Chang et al., "High reduction of interfacial charge recombination in colloidal quantum dot solar cells by metal oxide surface passivation," *Nanoscale* **7**, 5446–5456 (2015).

140. H. Wang et al., "PbS colloidal quantum dot/ZnO-based bulk-heterojunction solar cells with high stability under continuous light soaking," *Rapid Res. Lett.* **8**, 961–965 (2014).

141. H. Wang et al., "Enhanced carrier transport distance in colloidal PbS quantum-dot-based solar cells using ZnO nanowires," *J. Phys. Chem. C* **119**, 27265–27274 (2015).

142. T. Kawawaki et al., "Efficiency enhancement of PbS quantum dot/ZnO nanowire bulk-heterojunction solar cells by plasmonic silver nanocubes," *ACS Nano* **9**, 4165–4172 (2015).

143. K. S. Leschkies et al., "Solar cells based on junctions between colloidal PbSe nanocrystals and thin ZnO films," *ACS Nano* **3**, 3638–3648 (2009).

144. K. S. Leschkies et al., "Nanowire-quantum-dot solar cells and the influence of nanowire length on the charge collection efficiency," *Appl. Phys. Lett.* **95**, 193103 (2009).

145. J. Gao et al., "Quantum dot size dependent J-V characteristics in heterojunction ZnO/PbS quantum dot solar cells," *Nano Lett.* **11**, 1002–1008 (2011).

146. J. Tang et al., "Colloidal-quantum-dot photovoltaics using atomic-ligand passivation," *Nat. Mater.* **10**, 765–771 (2011).

147. I. H. Ip et al., "Hybrid passivated colloidal quantum dot solids," *Nat. Nanotechnol.* **7**, 577–582 (2012).

148. J. Zhang et al., "PbSe quantum dot solar cells with more than 6% efficiency fabricated in ambient atmosphere," *Nano Lett.* **14**, 6010–6015 (2014).

149. S. Kim et al., "Air-stable and efficient PbSe quantum-dot Solar cells based upon ZnSe to PbSe cation-exchanged quantum dots," *ACS Nano* **9**, 8157–8164 (2015).

150. R. Brown et al., "Energy level modification in lead sulfide quantum dot thin films through ligand exchange," *ACS Nano* **8**, 5863–5872 (2014).

151. C.-H. M. Chuang et al., "Improved performance and stability in quantum dot solar cells through band alignment engineering," *Nat. Mater.* **13**, 796–801 (2014).

152. Y. Cao et al., "The role of surface passivation for efficient and photostable PbS quantum dot solar cells," *Nat. Energy* **1**, 16035 (2016).

153. R. Azmi et al., "High-efficiency colloidal quantum dot photovoltaic devices using chemically modified heterojunctions," *ACS Energy Lett.* **1**, 100–106 (2016).

154. G.-H. Kim et al., "Correction to high-efficiency colloidal quantum dot photovoltaics via robust self-assembled monolayers," *Nano Lett.* **16**, 822–822 (2016).

155. D. Schaller and V. I. Klimov, "High efficiency carrier multiplication in PbSe nanocrystals: implications for solar energy conversion," *Phys. Rev. Lett.* **92**, 186601 (2004).

156. M. C. Beard et al., "Multiple exciton generation in colloidal silicon nanocrystals," *Nano Lett.* **7**, 2506–2512 (2007).

157. J. E. Murphy et al., "PbTe colloidal nanocrystals: synthesis, characterization, and multiple exciton generation," *J. Am. Chem. Soc.* **128**, 3241–3247 (2006).

158. Z. Lin, A. Franceschetti, and M. T. Lusk, "Size dependence of the multiple exciton generation rate in CdSe quantum dots," *ACS Nano* **5**, 2503–2511 (2011).

159. Q. Shen et al., "Ultrafast carrier dynamics in PbS quantum dots," *Chem. Phys. Lett.* **542**, 89–93 (2012).

160. V. Kershaw et al., "Multiple exciton generation in cluster-free alloy $Cd_xHg_{1-x}Te$ colloidal quantum dots synthesized in water," *Phys. Chem. Chem. Phys.* **16**, 25710–25722 (2014).

161. O. E. Semonin et al., "Peak external photocurrent quantum efficiency exceeding 100% via MEG in a quantum dot solar cell," *Science* **334**, 1530–1533 (2011).

162. A. Jackson Stolleb et al., "Multiexciton solar cells of CuInSe nanocrystals," *J. Phys. Chem. Lett.* **5**, 304–309 (2014).

163. N. L. K. Davis et al., "Multiple-exciton generation in lead selenide nanorod solar cells with external quantum efficiencies exceeding 120%," *Nat. Commun.* **6**, 8259 (2015).

164. H. Zhu et al., "Auger-assisted electron transfer from photoexcited semiconducot quantum dots," *Nano Lett.* **14**, 1263–1269 (2014).

165. J. H. Olshansky, "Hole transfer from photoexcited quantum dots: the relationship between driving force and rate," *J. Am. Chem. Soc.* **137**, 15567–15575 (2015).

Biographies for the authors are not available.